



**HAL**  
open science

## Detection and characterization of VIM-52, a new variant of VIM-1 from *Klebsiella pneumoniae* clinical isolate

Marie de Barsy, Paola Sandra Mercuri, Saoussen Oueslati, Eddy Elisée, Te-Din Huang, Pierre Sacré, Bogdan Iorga, Thierry Naas, Moreno Galleni, Pierre Bogaerts

### ► To cite this version:

Marie de Barsy, Paola Sandra Mercuri, Saoussen Oueslati, Eddy Elisée, Te-Din Huang, et al.. Detection and characterization of VIM-52, a new variant of VIM-1 from *Klebsiella pneumoniae* clinical isolate. *Antimicrobial Agents and Chemotherapy*, 2021, 65 (11), pp.e02660-20. 10.1128/aac.02660-20. hal-03336206

**HAL Id: hal-03336206**

**<https://hal.science/hal-03336206>**

Submitted on 7 Sep 2021

**HAL** is a multi-disciplinary open access archive for the deposit and dissemination of scientific research documents, whether they are published or not. The documents may come from teaching and research institutions in France or abroad, or from public or private research centers.

L'archive ouverte pluridisciplinaire **HAL**, est destinée au dépôt et à la diffusion de documents scientifiques de niveau recherche, publiés ou non, émanant des établissements d'enseignement et de recherche français ou étrangers, des laboratoires publics ou privés.

1 **Detection and characterization of VIM-52, a new variant of VIM-1 from**  
2 ***Klebsiella pneumoniae* clinical isolate**

3 Marie de Barsy<sup>a</sup>, Paola Sandra Mercuri<sup>b</sup>, Saoussen Oueslati<sup>c,d,e</sup>, Eddy Elisée<sup>f</sup>, Te-Din Huang<sup>a</sup>,  
4 Pierre Sacré<sup>a</sup>, Bogdan I. Iorga<sup>f</sup>, Thierry Naas<sup>c,d,e</sup>, Moreno Galleni<sup>b</sup>, Pierre Bogaerts<sup>a</sup>

5 <sup>a</sup>Laboratory of Bacteriology, CHU UCL Namur, Université Catholique de Louvain, Yvoir,  
6 Belgium

7 <sup>b</sup>InBios-Laboratoire de Macromolécules Biologiques, Centre d'Ingénierie des Protéines,  
8 Université de Liège, Liège, Belgium.

9 <sup>c</sup>Team ReSIST, INSERM U1184, School of Medicine Université Paris-Saclay, LabEx  
10 LERMIT, Le Kremlin-Bicêtre, France

11 <sup>d</sup> Bacteriology-Hygiene unit and French National Reference Center for Antibiotic Resistance:  
12 Carbapenemase-producing Enterobacteriaceae, Assistance Publique/Hôpitaux de Paris,  
13 Bicêtre Hospital, Le Kremlin-Bicêtre, France

14 <sup>e</sup> Evolution and Ecology of Resistance to Antibiotics Unit, Institut Pasteur – APHP -  
15 Université Paris-Sud, Paris, France

16 <sup>f</sup>Université Paris-Saclay, CNRS, Institut de Chimie des Substances Naturelles, Gif-sur-Yvette,  
17 France

18  
19 **KEYWORD :** antibiotic resistance, metallo- $\beta$ -lactamase, *Klebsiella pneumoniae*,  
20 biochemical characterization

21 **Abstract: 139**

22 **Text: 4688**

23 **Figures: 6**

24 **Tables: 4**

25 **Supplementary material: 3**

26  
27 Corresponding author: Pierre Bogaerts, CHU UCL Namur, Av Dr Gaston Thérassé, 1 à 5530  
28 Yvoir. Email: [pierre.bogaerts@uclouvain.be](mailto:pierre.bogaerts@uclouvain.be); Tel: +32 81 423241

29  
30  
31  
32 **ABSTRACT**

33 Over the last two decades, antimicrobial resistance has become a global health problem. In  
34 Gram-negative bacteria, metallo- $\beta$ -lactamases (MBLs), which inactivate virtually all  $\beta$ -  
35 lactams, increasingly contribute to this phenomenon. The aim of this study is to characterize  
36 VIM-52, a His224Arg variant of VIM-1, identified in a *Klebsiella pneumoniae* clinical isolate.  
37 VIM-52 conferred lower MICs to cefepime and ceftazidime as compared to VIM-1. These  
38 results were confirmed by steady state kinetic measurements, where VIM-52 yielded a lower  
39 activity towards ceftazidime and cefepime but not against carbapenems. Residue 224 is part  
40 of the L10 loop (residues 221-241), which borders the active site. As Arg 224 and Ser 228 are  
41 both playing an important and interrelated role in enzymatic activity, stability and substrate  
42 specificity for the MBLs, targeted mutagenesis at both positions were performed and further  
43 confirmed their crucial role for substrate specificity.

44

## 45 INTRODUCTION

46 Multidrug-resistance in Gram-negative bacteria represents a major public health problem (1).  
47 The emergence and spread of acquired carbapenemases such as metallo- $\beta$ -lactamases (MBLs)  
48 are of particular concern (2). MBLs were first reported in 1966, and were initially not  
49 considered as a serious threat for antimicrobial chemotherapy as they were mostly  
50 chromosomally-encoded in non-pathogenic bacteria (3). The situation is now different, as the  
51 genes encoding MBLs are frequently located on mobile genetic structures facilitating  
52 dissemination and spread among clinically-relevant Gram-negative bacteria (4, 5). The MBLs  
53 are divided in three subclasses, B1, B2 and B3. The most important acquired MBLs are  
54 members of subclass B1 as Verona Integron-encoded Metallo- $\beta$ -lactamase (VIM) (6) and  
55 New Delhi Metallo- $\beta$ -lactamase (NDM) (7). *Bla*<sub>VIM-1</sub> was first identified as a chromosomally  
56 encoded within a class I integron in a *Pseudomonas aeruginosa* clinical isolate (6). Today,  
57 VIM-1-like enzymes are mostly identified in multidrug-resistant Enterobacterales species (4,  
58 5). VIM enzyme family currently includes 73 different variants (<http://www.blddb.eu/> ; (8))  
59 divided in 5 different clusters of closely sequence-related enzymes namely VIM-1, VIM-2  
60 (the 2 major clusters) and VIM-7, VIM-12 and VIM-13 variants (9). Similar to other MBLs,  
61 VIM enzymes hydrolyze all  $\beta$ -lactams with the exception of monobactams. Their fold forms a  
62  $\alpha\beta\beta\alpha$  sandwich and their active site is located in a central groove on one edge of the two  
63  $\beta$  sheets. The active site is able to bind two zinc ions, positioned respectively in the  
64 tetrahedral Zn1 site- formed by the conserved H116, 118 and 196- and the Zn2 site including  
65 D120, C221 and H263 [BBL numbering scheme, (10-14) ]. Amino-acids at position 224 and  
66 228 are part of the L10 loop (residues 221-241) located near the active site. Compared to the  
67 other subclass B1 MBLs (NDM-1 and IMP-1) which harbored a positively charged lysine at  
68 position 224, VIM enzymes display a histidine (VIM-1 variants) or a tyrosine (VIM-2  
69 variants) with the exception of VIM-26 and VIM-28 (Leucine 224) which abolish the

70 presence of a positive charge near the active site. This affects the interaction of VIM enzymes  
71 with the conserved carboxylic function of the  $\beta$ -lactam compounds and its intrinsic stability  
72 (15, 16). The presence of an arginine at position 228 can structurally replace the function of  
73 the Lys 224 (17) but most of the variants containing an Arg 228, such as VIM-4, displays a  
74 lower hydrolysis efficiency against expanded-spectrum cephalosporins. Within the VIM-1  
75 subgroup, the presence of a serine at position 228 increases the accessibility of the active site  
76 and its activity towards substrates with bulky side chains in C3 like the third-and/or fourth  
77 generation cephalosporins. We report here the characterization of VIM-52-producing *K.*  
78 *pneumoniae* clinical isolate (*Kp\_20150593*) and of the kinetic parameters of the purified  
79 VIM-52 protein. VIM-52 differed from VIM-1 by a single histidine to arginine substitution at  
80 position 224. Due to the importance of the residue at position 224 and 228, we generated  
81 different mutants of VIM-1 (H224A, H224D, H224K) and VIM-52 (S228A, S228D, S228K,  
82 S228R) to explore their influence on the structure of the L10 loop, the active site and the VIM  
83 substrate specificity. The rationale behind these choices was to replace the existing amino-  
84 acids (AA) by a small neutral AA (Alanine), a positively charged amino acid (Lysine) and a  
85 negatively charged AA (Aspartate). In addition, for VIM-52, we further replace the S228 (a  
86 polar AA) by the positively charged R in order to explore the effect of the potential steric and  
87 charge hindrance of the 2 arginines at position 224 and 228. Three dimensional modeling and  
88 molecular dynamics simulation were also performed.

## 89 **RESULTS**

### 90 **VIM-52, a single AA variant of VIM-1: clinical context and molecular identification**

91 A 67-year-old Belgian patient developed a severe acute respiratory distress episode during a  
92 holiday stay in Greece and was hospitalized in a local intensive care unit (ICU) requiring  
93 intubation and mechanical ventilation. Three days later he was repatriated to the ICU of a  
94 general hospital in Belgium where microbiological samples collected from several anatomical  
95 sites (sputum, rectal swab and urine) cultured a carbapenem-resistant *K. pneumoniae* isolate

96 (*Kp*\_20150593). The isolate displayed high-level resistance to penicillins, third-generation  
97 cephalosporins and carbapenems but remained susceptible to cefepime and to aztreonam  
98 (Table 1).

99 In house multiplex PCR confirmed the presence of a *bla*<sub>VIM</sub> gene and subsequent Sanger  
100 sequencing revealed a *bla*<sub>VIM-52</sub> allele, a novel single AA variant H224R of VIM-1 (Figure  
101 1A).

102 Whole genome sequencing (WGS) of the VIM-52-producing *Kp*\_20150593 revealed that  
103 *Kp*\_20150593 belonged to the ST147 and capsula r-type KL64 type. VIM-1-producing *K.*  
104 *pneumoniae* ST147 have been reported previously in several hospital in Greece (18) and *K.*  
105 *pneumoniae* ST147 is considered as an emerging high-risk clone harboring different  
106 carbapenemases and responsible of hospital outbreaks all over Europe (19, 20). To the best of  
107 our knowledge, no other case of VIM-52 producing isolates has been reported.

108 The *bla*<sub>VIM-52</sub> gene is located on a 5,884 bp contig presenting a Blast best hits (query cover  
109 100%, E value 0.0, percentage identity 99.97%) with a region of the plasmid pIncRIncN from  
110 *K. pneumoniae* strain 1\_GR\_13 (CP027047.1) harboring *bla*<sub>VIM-27</sub> gene (data not shown). The  
111 *bla*<sub>VIM-52</sub> gene is embedded in a class I integron together with two additional gene cassettes  
112 conferring resistance to aminoglycoside (*aac*(6')-I and *aph*(3'')-Ia) and one to trimethoprim  
113 (*dhfr*AI) (Figure 1B). The *bla*<sub>VIM-52</sub> gene cassette is inserted at the first position of the variable  
114 region of the integron, immediately downstream to the integron borne strong promoter Pc  
115 (Figure 1B).

116 A ~50 kb plasmid was extracted from *Kp*\_20150593 by the Kieser method. This plasmid was  
117 electroporated to *E. coli* Top10 and mating-out experiment using J53 azide-resistant *E. coli* as  
118 recipient strain confirmed that pIncRIncN-VIM-52 is a self-conjugative plasmid. The  
119 transconjugant and the transformant displayed a similar antimicrobial resistance profile which  
120 was different from the parental *Kp*\_20150593 isolate (Table 1) indicating that resistance to

121 ciprofloxacin, colistin and fosfomycin are not related to the VIM-52 plasmid. The  
122 mechanisms of resistance to these antibiotics will not be investigated in the present study.

123 **Site directed mutagenesis of H224 and S228 amino acids in VIM-1 and VIM-52,**  
124 **respectively.**

125 The MIC of *E. coli* producing VIM-1 and variants against different beta-lactam antibiotics  
126 (Figure 2) were determined by broth microdilution (Table 2). Compared to VIM-1, the natural  
127 H224R substitution in VIM-52 conferred a very similar resistance profile to carbapenems and  
128 most  $\beta$ -lactams (no more than 1 dilution difference, Table 2). Nevertheless, for ceftazidime, a  
129 difference of at least two dilutions was detected ( $>128$  to  $64 \mu\text{g/mL}$  for VIM-1 and VIM-52,  
130 respectively) and for cefepime, a dramatic drop of MIC value was observed (from  $64$  to  $0.25$   
131  $\mu\text{g/mL}$ ) suggesting an almost complete loss of cefepime hydrolysis by VIM-52.

132 In other VIM-1 variants at position 224, such as H224D, an increase of the susceptibility to  
133 ertapenem was observed ( $0.25 \mu\text{g/mL}$  instead of  $1 \mu\text{g/mL}$  for VIM-1), while mutation H224K  
134 increased the susceptibility to meropenem ( $1 \mu\text{g/mL}$  instead of  $4 \mu\text{g/mL}$  for VIM-1).  
135 Nevertheless, the most dramatic effect was observed with cefepime (Table 2) for which the  
136 resistance profile ranged from  $64 \mu\text{g/mL}$  for VIM-1 to  $0.25 \mu\text{g/mL}$  for VIM-52 with a gradual  
137 increase of the susceptibility according to the nature of the mutation at position 224 (MIC of  
138 VIM-1  $>$  H224A  $>$  H224D  $>$  H224K  $>$  H224R [VIM-52]).

139 Mutations performed on VIM-52 at position 228, such as S228A and S228K had minor effect  
140 on MIC values, while S228R, led to an additional decreased resistance to meropenem as  
141 compared to VIM-52. On the contrary, S228D mutations restored partially resistance  
142 phenotype to cefepime ( $2 \mu\text{g/mL}$ ) while susceptibility to ertapenem was increased ( $0.25$   
143  $\mu\text{g/mL}$ ) (Table 2).

144 Four representative mutants (VIM-1 H224K; VIM-52 [H224R], VIM-52 S228D and S228R)  
145 were further studied by molecular modelling and purified to homogeneity in order to  
146 determine their hydrolytic parameters.

#### 147 **Structural analysis of the VIM variants**

148 A three-dimensional model was constructed for each of these VIM variants starting from the  
149 crystal structure of VIM-1 (PDB code 5N5I) (16) then submitted to molecular dynamics  
150 (MD) simulations, which reached very quickly an equilibrium, with root-mean-square  
151 deviation (RMSD) values of about 1 Å that were conserved throughout (Figure S1). Each  
152 mutant features a specific conformation of the loop L10 (residues 221-241) (Figure S2) and a  
153 specific shape of the binding site (Figure 3). The hydrogen bond interactions that are  
154 controlling the conformation of the loop L10 are presented in Figure 4. The hydrogen bonds  
155 between the side chain of T275 and the backbone of the residues in position 224, as well as  
156 between the side chain of H274 and the backbone of the residue in position 228, are present in  
157 all six VIM variants studied, with the exception of K224/S228 (Figure 4b) where H274 is  
158 absent. Additional hydrogen bonds were observed in these mutants, all of them constituting  
159 essential elements to define the conformation of the L10 loop (Figure 4).

#### 160 **Steady-state kinetic analysis**

161 Table 3 shows that VIM-52 displayed higher catalytic efficiencies ( $k_{\text{cat}}/K_m$ ) towards  
162 benzylpenicillin, and cefotaxime as compared to VIM-1 but lower towards ceftazidime and  
163 cefepime while remaining similar toward imipenem and meropenem. Also,  $k_{\text{cat}}$  values for  
164 meropenem and ertapenem ( $0.3 \text{ s}^{-1}$ ) were lower than the  $k_{\text{cat}}$  for imipenem ( $2.2 \text{ s}^{-1}$ ). This  
165 suggests that the active site of VIM-52, because of the presence of the large positively  
166 charged R224, is less able to interact with bulky and/or positively charged C3 substrates  
167 (Figure 2). Indeed, cephalothin and cefotaxime, which possess the same small uncharged C3  
168 acetoxymethyl group substituent, are hydrolyzed with the same efficiency (Table 3) although

169 cefotaxime possesses a larger C7-lateral chain ([2-(2-amino-1,3-thiazol-4-yl)-2-  
170 (methoxyimino) acetyl] amino group instead of the 2-thienylacetyl nitrilo group for  
171 cephalothin. Interestingly, the only structural difference between cefepime and cefotaxime is  
172 the presence of a bulky and positively charged C3 lateral chain (1-methylpyrrolidinium-1-  
173 methyl group) in cefepime instead of the small acetoxymethyl group for cefotaxime (Figure  
174 2). The presence of this group results in a reduced affinity (increase in  $K_m$  value) for cefepime  
175 as compared to cefotaxime and thus a large reduction of the VIM-52 catalytic efficiency. The  
176 same observation can be made with ceftazidime that also presents a bulky and positively  
177 charged C3 substituent (*N*-methyl-pyridinium group). For these  $\beta$ -lactams, we noted more  
178 than 10-fold increase in the  $K_m$  values as compared to cephalothin or cefotaxime. Therefore,  
179 we were not able to measure  $k_{cat}$  and  $K_m$  independently since, in our experimental conditions,  
180 their hydrolysis were characterized by a first-order kinetic. Molecular docking calculations of  
181 cefotaxime with the R224/S228 variant provided a possible explanation for these results,  
182 showing a binding mode with hydrogen bonds of the side chain of R224 with the carboxylate  
183 group and with the carbonyl oxygen of the ester group of cefotaxime (Figure 5a). The binding  
184 modes of cefepime (Figure 5b) or ceftazidime are slightly different due to repulsive  
185 interactions between the side chain of R224 and the positively charged substituents in position  
186 C3, thus explaining the higher  $K_m$  values determined experimentally for these two molecules.  
187 With its small and neutral substituent in C3, cephalothin remains a good substrate for both  
188 VIM-1 and VIM-52 MBLs.

189 VIM-52 and VIM-1 displayed a similar catalytic efficiency ( $k_{cat}/K_m$ ) towards carbapenems.  
190 Nevertheless,  $k_{cat}$  and  $K_m$  for meropenem were strongly reduced as compared to VIM-1. These  
191 results suggested different modes of interaction of meropenem with the active site residues.  
192 Molecular docking calculations on the R224/R228 variant showed strong hydrogen bonds  
193 between the carboxylate group of meropenem and the side chain of R224 in VIM-52, which

194 are not possible with the shorter side chain of H224 in VIM-1 (Figure 6a). A similar  
195 explanation was found for benzylpenicillin, which is a better substrate for VIM-52 (Figure  
196 6b). If we compare the enzyme activities towards third and fourth generation cephalosporins,  
197 we can note that cefotaxime was a better substrate for VIM-52 ( $k_{\text{cat}}/K_m$  for VIM-52 is 5 times  
198 higher). In contrast, VIM-52 was less active against cefepime and ceftazidime than VIM-1,  
199 with a ratio of  $k_{\text{cat}}/K_m$  for VIM-52 and VIM-1 of 0.026 and 0.15, respectively. These latter  
200 observations are in agreement with the MIC determined for *E. coli* TOP10 producing VIM-1  
201 or VIM-52 (Table 2). This confirmed that the presence of an arginine in position 224 is less  
202 favorable to accommodate the positively charged C3-N-methyl pyrrolidine group of the  
203 cepheems (Figure 5). Furthermore, the H224K VIM-1 variant showed about 100 times reduced  
204 activity towards cefepime (ratio of  $k_{\text{cat}}/K_m$  for H224K VIM-1 and that for VIM-1 was 0.007).  
205 Interestingly, the H224K VIM-1 mutant was more active against benzylpenicillin, cefotaxime  
206 and imipenem and meropenem (ratios of 123, 8, 7.7 and 30, respectively) (Table 3). The  
207 presence of a lysine at position 224 enhances the catalytic efficiency toward carbapenems and  
208 benzylpenicillin but does not explain MICs against carbapenems (Table 2). This discrepancy  
209 might suggest a lower level of expression and/or stability of this mutant which is supported by  
210 the western blot experiments showing a lower signal for VIM-1 H224K mutant than for VIM-  
211 1 (Figure S3). This experimental observation might explain why H224K has never been  
212 identified while being more active against carbapenems than H224R (VIM-52).

213 We also explored the function of the amino acid 228 in VIM-52. Our data showed that the  
214 S228D VIM-52 mutant was more or equally efficient against all the tested substrates as  
215 compared to the VIM-52 (Table 4 R4-VIM-52 ratio). This phenomenon was mainly due to the  
216 increase of the  $k_{\text{cat}}$  values. Interestingly, the catalytic efficiency of VIM-52 S228R against  
217 ceftazidime and cefepime dropped as compared to VIM-52, mainly due to the lower  $k_{\text{cat}}$  of the  
218 mutant. On the other hand, activity against carbapenems of this mutant rose due to higher  $k_{\text{cat}}$

219 for imipenem ( $20 \text{ s}^{-1}$  instead of  $2.2 \text{ s}^{-1}$  for VIM-52) and a decrease of  $K_m$  for meropenem (0.03  
220  $\mu\text{M}$  instead of  $0.7 \mu\text{M}$  for VIM-52) and ertapenem ( $0.06 \mu\text{M}$  instead of  $0.5 \mu\text{M}$  for VIM-52)  
221 with  $k_{\text{cat}}$  remaining roughly unchanged (Table 4). The analysis of the enzymatic profile of the  
222 double R224 R228 mutant compared to VIM-1 showed a major drop in activity against  
223 ceftazidime and cefepime due to the decrease of the  $k_{\text{cat}}$  value and a higher catalytic efficiency  
224 against cefotaxime and carbapenems.

225

## 226 **DISCUSSION**

227 As MBLs are increasingly spreading in Gram-negative bacteria, novel variants of known  
228 MBLs with altered substrate specificities will be discovered. Here, we have characterized  
229 phenotypically and biochemically VIM-52, a novel H224R VIM-1 variant present in a clinical  
230 isolate of *K. pneumoniae* belonging to ST147. The  $bla_{\text{VIM-52}}$  gene was embedded in a class I  
231 integron carried by a 50-kb size IncR-IncF plasmid, whose sequence is highly similar to a  
232 plasmid sequence (accession number NZ\_CP027047.1) found in a *K. pneumoniae* strain  
233 1\_GR\_13 belonging also to ST147 (21), isolated from a Greek patient in 2013. Thus, it is  
234 likely that the patient acquired *Kp*\_20150593 during his hospital stay in Greece.

235 Constitutive expression of the  $bla_{\text{VIM-52}}$  gene in *E. coli* TOP10, suggested that VIM-52 is a  
236 carbapenemase with impaired cefepime hydrolysis (MIC =  $0.25 \mu\text{g/mL}$ ) as compared to VIM-  
237 1 (MIC =  $64 \mu\text{g/mL}$ ). Steady state kinetic parameters confirmed phenotypical observation and  
238 revealed for VIM-52 a nearly 40 fold lower activity against cefepime as compared to VIM-1.  
239 These results are in line with a recent publication that compared the MIC values of VIM-1  
240 and VIM-52 (22). While they observed that the H224R mutation has no or poor effect on the  
241 level of carbapenem-resistance, they noticed a significant drop in MICs for ceftazidime (4-  
242 fold), similarly to what we observed, but they did not test cefepime.

243 Amino acids at position 224 and 228 are known to be important for substrate binding (17). In  
244 order to further explore the amino acid specificities at these positions we prepared several

245 point mutant derivatives by directed mutagenesis. We were able to show that the presence of  
246 an arginine at position 228 affects the substrate profile, i.e. an increased catalytic efficiency  
247 against imipenem and meropenem and a decreased catalytic efficiency against cefepime and  
248 ceftazidime (Table 4). This is in agreement with the activity profile of VIM-13 and VIM-19,  
249 respectively (23, 24).

250 In many subclass B1 (5, 25) and B2 (12) MBLs, the conserved Lys residue at position 224,  
251 close to the active site, plays an important role in substrate binding (17). In the case of VIM  
252 enzymes, K224 is substituted by H224 in VIM-1 and by Y224 in VIM-2. The shorter side  
253 chain of histidine and the uncharged lateral chain of tyrosine prevent the interaction of these  
254 two amino acids with the carboxylate moiety (C4 or C3) of the substrate. The presence of  
255 K224 allows the interaction with the substrate but also creates a stronger interaction with  $\alpha$ -  
256 carbonyl moiety of the main chain of A231 and the water molecule shared with H196. This  
257 mutation favours a better docking of the antibiotic in the active site pocket and the  
258 polarization of the water molecule may increase the acid Lewis strength of the Zn<sup>2+</sup> and its  
259 hydrolytic activity (26). On the other hand, the presence of K224, resulted in a decrease of the  
260  $k_{cat}$  and an increase of the  $K_m$  value for cefepime, which resulted in a sharp decrease of the  
261 catalytic efficiency as compared to VIM-1 (R2 ratio for cefepime = 0.007) (Table 3). We  
262 noticed that the catalytic efficiency of this VIM-1 H224K mutant is enhanced for cefotaxime  
263 (R2 ratio for cefotaxime = 8). Knowing that the only difference between cefotaxime and  
264 cefepime structure is the nature of the C3 lateral chain, our hypothesis is that the presence of a  
265 bulky and positively charged C3 lateral chain of cefepime affected its positioning in the active site and  
266 therefore its hydrolysis by the MBL.

267 It was hypothesized that R228 (17), may act as stabilizer of carbapenems in the catalytic  
268 pocket of the MBLs. This seems confirmed by the observation of the activity enhancement  
269 against carbapenems of the VIM-52 S228R (from 11 to 460 fold compared to VIM-52, VIM-1

270 or VIM-2). On the contrary, we confirmed that the substitution of S228 in arginine  
271 dramatically lower the activity against ceftazidime and cefepime while not against  
272 cefotaxime. Our data underline the importance of the large positively charged C3 especially  
273 when position 224 and 228 are both positively charged (R). The presence of the lateral chain  
274 of arginine induced steric clashes and hindrance compromising the hydrolysis of cefepime  
275 and ceftazidime.

276 Interestingly, with the mutation H224K VIM-1 (S228) we also observed an increased catalytic  
277 efficiency against imipenem and meropenem and a decreased catalytic efficiency against  
278 cefepime and ceftazidime as in S228R VIM-52. This further suggests that R228 could replace  
279 the K224 for substrates binding and confirmed the importance of residues 224 and 228 for the  
280 carbapenemase activity in MBL (13, 14, 25).

281

## 282 **MATERIALS AND METHODS**

### 283 *Antibiotics*

284 Kanamycin was purchased from MP Biomedicals, France. Chloramphenicol, benzylpenicillin,  
285 cephalotin, cefotaxime and ceftazidime were purchased from Sigma Aldrich, (Overijse,  
286 Belgium). Cefepime was a gift from Fresenius Kabi, (Schelle, Belgium). Imipenem and  
287 ertapenem were purchased from MSD, (Brussels, Belgium) and meropenem from  
288 AstraZeneca (Dilbeek, Belgium).

### 289 *Bacterial isolates*

290 The clinical strain *Kp\_20150593* expressing the VIM-52- $\beta$ -lactamase was used for cloning of  
291 the *bla*<sub>VIM-52</sub> gene. *E. coli* TOP10 (Invitrogen, Saint-Aubin, France) and Stellar *E. coli*  
292 competent cells (Invitrogen, Merelbeke, Belgium) were used for cloning, azide resistant *E.*  
293 *coli* J53 for conjugation experiments and *E. coli* Rosetta (DE3) (Novagen, Fontenay-sous-  
294 Bois, France) for overexpression experiments.

### 295 *Bacterial identification, antimicrobial susceptibility testing and carbapenemase detection*

296 Bacterial identification to the species level was performed using MALDI-TOF mass  
297 spectrometry (MALDI Biotyper; Bruker Daltonics, Bremen, Germany).

298 Antimicrobial susceptibility testing was determined by disc diffusion on Mueller-Hinton agar  
299 plates (BioRad, Marnes-La-Coquette, France) according to the CLSI guidelines (CLSI M-  
300 100-S15). MIC values were determined by broth microdilution using Sensititre plates (Trek  
301 Diagnostic Systems, Cleveland, OH, USA).

302 The carbapenemase activity was assessed by a biochemical (Rapidec, bioMérieux, Marcy-l-  
303 Etoile, France) and electrochemical BYG tests (27). The carbapenemase gene was detected by  
304 an in-house PCR ISO15189 certified. PCR products were subsequently Sanger sequenced by  
305 an external sequencing provider (Macrogen, Seoul, Korea) (28).

306

#### 307 *Plasmid analysis, conjugation and transformation assays*

308 Plasmid DNA was extracted from *Kp\_20150593* by the Kieser method and analyzed by 0.7%  
309 agarose gel electrophoresis using as a plasmid size marker the plasmid extract of the *E. coli*  
310 NCTC50192, which harbors four plasmids of 154, 66, 48, and 7 kb. The plasmid extract of  
311 *Kp\_20150593* was used to transform *E. coli* TOP10 by electroporation using the Gene Pulser  
312 II apparatus. Transformants were selected on LB agar plates containing 100 µg/mL of  
313 ampicillin. Solid mating experiment was performed using *E. coli* J53 (azide resistant) as  
314 recipient strain. The transconjugants were selected on LB agar plate containing 100 µg/mL of  
315 azide and 100 µg/mL of ampicillin. Transformants and transconjugants were tested by disk  
316 diffusion and broth microdilution antibiograms and colony PCR using primers targeting the  
317 *bla*<sub>VIM</sub> gene (29).

318

#### 319 *Whole genome sequencing*

320 Genomic DNA was extracted using NucliSENS® easyMag® (bioMérieux, Marcy-l’Etoile,  
321 France), following manufacturer’s instructions. Dual-indexed Illumina sequencing library was  
322 constructed using Nextera DNA Flex library preparation (Illumina Inc, CA, USA). Libraries  
323 were pooled and 100 pM were sequenced on the Illumina iSeq100 (2x150 bp). Sequence  
324 quality was assessed by FastQC. Reads were trimmed using Trimmomatic. Genome assembly  
325 was performed using Spades and assembly quality was assessed using Quast. Resistance  
326 genes and replicons were identified using ResFinder  
327 (<https://cge.cbs.dtu.dk/services/ResFinder/>) and PlasmidFinder  
328 (<https://cge.cbs.dtu.dk/services/PlasmidFinder/>), respectively. The contig #38 harboring  
329 *bla*<sub>VIM-52</sub> gene (accession number GenBank: ANI25016.1) was annotated using RAST  
330 (<http://rast.theseed.org/FIG/rast.cgi>), Integrall (<http://integrall.bio.ua.pt/>) and ISFinder  
331 (<https://isfinder.biotoul.fr/blast.php>). The contig #38 sequence was aligned against *K.*  
332 *pneumoniae* (TaxID 573) using NCBI Blast tool. Multi Locus sequence type (MLST) was  
333 determined using BIGSdb-Kp Pasteur database, while capsular-type using Kaptive webtool  
334 (<http://kaptive.holtlab.net/>)

335

### 336 ***Site-directed mutagenesis, cloning and expression***

337 *Bla*<sub>VIM-1</sub> and *bla*<sub>VIM-52</sub> genes and their ribosome binding site (RBS) were amplified using Q5®  
338 High-Fidelity DNA polymerase (Bioké, Leiden, The Netherlands) and ligated into the pCR-  
339 Blunt II-TOPO vector according to manufacturer’s instruction (ThermoFisher, Brussels,  
340 Belgium). Ligation products were used to transform *E. coli* TOP10 by electroporation and  
341 transformants selected on LB containing 50µg/mL kanamycin. Colonies were screened by  
342 PCR using M13 Forward (-20) and M13 reverse universal primers. Amplified DNA were  
343 sequenced by an external DNA sequencing service (Macrogen Inc., Seoul, South Korea) using  
344 the same primers to check sequence and orientation of the inserted fragment.

345 These two plasmids pTOPO-VIM-1 and pTOPO-VIM-52 were used for PCR site-directed  
346 mutagenesis using QuickChange II Site-Directed Mutagenesis Kit according to the  
347 manufacturer recommendation (Agilent Technologies, Diegem, Belgium) to obtain the  
348 following variants: VIM-1 H224A, H224D, H224K; VIM-52 S228A, S228D, S228K, S228R  
349 and were ligated into the pCR-Blunt II-TOPO. The MIC values of all the *E. coli* TOP10  
350 strains expressing constitutively VIM-1 and VIM-52 and their mutants were determined by  
351 broth microdilution as described above.

352

### 353 ***Protein production and purification***

354 *Bla*<sub>VIM-1</sub>, and *bla*<sub>VIM-52</sub> genes and their variants were amplified using Q5® High-Fidelity DNA  
355 polymerase and introduced into the pET26b plasmid using the In-Fusion HD cloning kit  
356 (Takara bio, Saint-Germain-en-Laye, France), following the manufacturer's instruction. The  
357 In-Fusion reaction mixtures were used to transform Stellar *E. coli* competent cells and  
358 transformants were selected on LB containing 50 µg/mL kanamycin. Colonies were screened  
359 by PCR using T7 primers. All the enzymes were produced in *E. coli* Rosetta (DE3) carrying  
360 pET26b/*bla*<sub>VIM-52</sub>, pET26b/*bla*<sub>VIM-1</sub> and mutants thereof. The cultures were performed in LB  
361 medium supplemented with kanamycin (50 µg/mL) and chloramphenicol (30 µg/mL). The  
362 cultures were incubated O/N at 37°C under agitation and 40 mL were used to inoculated 1  
363 Liter of fresh LB medium supplemented as described above. IPTG (50 µM final  
364 concentration) was added when the culture reached to an optical density at 600 nm of 0.7 and  
365 then the cultures were incubated O/N at 18°C. Cells were harvested by centrifugation (5,000 g  
366 for 10 min at 4°C), and the pellets were resuspended in 40 mL of 50 mM MES buffer pH 6.5,  
367 50 µM ZnCl<sub>2</sub> (buffer A). The bacteria were disrupted with the help of a cell disrupter  
368 (Emulsiflex C3; Avestin GmbH, Germany), which allows cell lysis at a pressure of 5.500 kPa.  
369 The lysates were centrifuged at 45,000 g for 30 min. The cleared supernatants were recovered

370 and filtered through a 45µm filter and was then loaded onto a Q Sepharose<sup>®</sup> HP (GE  
371 Healthcare, Machelen, Belgium) equilibrated with buffer A. The enzymes were eluted with a  
372 salt gradient using buffer A and 50 mM MES, pH 6.5 with 1 M NaCl, (buffer B). The  
373 fractions containing β-lactamase activity were pooled, and then dialyzed O/N in 25 mM  
374 HEPES, pH 7.5, 50 µM ZnCl<sub>2</sub>, 1.2 M (NH<sub>4</sub>)<sub>2</sub>SO<sub>4</sub>. The dialysed sample was loaded onto Butyl  
375 Sepharose High Performance (20 mL) (Pharmacia Biotech) previously equilibrated with 25  
376 mM HEPES, pH 7.5, 50 µM ZnCl<sub>2</sub>, 1.2M (NH<sub>4</sub>)<sub>2</sub>SO<sub>4</sub> (buffer A). The enzymes were eluted  
377 with a salt out gradient between buffer A and 25 mM HEPES, pH 7.5, 50 µM ZnCl<sub>2</sub> (buffer  
378 B). The active fractions were collected and concentrated on an YM-10 membrane (Amicon,  
379 Beverly, Mass.) to a final volume of 2 mL. The sample was loaded in a molecular sieve  
380 Superdex 75 GL (10/300) column (GE Healthcare, Belgium) equilibrated in 50 mM HEPES  
381 buffer pH 7.5, 50µM ZnCl<sub>2</sub> containing 0.2 M NaCl. At the end of each purifications step, β-  
382 lactamase activity was routinely measured spectrophotometrically by following the hydrolysis  
383 of a solution of 100 µM imipenem as previously described (14).

384 Steady-state kinetic parameters ( $K_m$  and  $k_{cat}$ ) were determined by measuring substrate  
385 hydrolysis under initial rate conditions and using the Hanes–Wolf linearization from the  
386 Michaelis–Menten equation (30). Kinetic experiments were performed by following the  
387 hydrolysis of each substrate at 30°C in 25 mM HEPES buffer pH 7.5, 50 µM ZnCl<sub>2</sub>. The data  
388 were collected with a Specord 50 PLUS spectrophotometer (Analytik, Jena, Germany). Each  
389 kinetic value is the mean of three different measurements.

390

### 391 ***Molecular modelling***

392 Three-dimensional structures of mutants were generated using the swapa command  
393 implemented in UCSF CHIMERA (31) starting from the structure of VIM-1 (PDB code  
394 5N5I) (16).

395 Molecular dynamics simulations were performed with GROMACS version 4.6.5 (32) using  
396 the OPLS-AA force field (33). The protein was centred in a cubic periodic box, with at least  
397 1.0 nm on each side. The simulation box was then filled with TIP4P water molecules and the  
398 system neutralized with Na<sup>+</sup> and Cl<sup>-</sup> ions until reaching the physiological ionic strength (150  
399 mM). Each system was energy-minimized until convergence using a steepest descents  
400 algorithm. Molecular dynamics with position restraints on backbone, with the exception of  
401 residues 223-232 which were unrestrained, was then performed for 50 ns. The  
402 Parrinello–Rahman method was used for pressure coupling (34) and the temperature was  
403 coupled using the Nosé–Hoover method at 300 K (35, 36). Electrostatics were calculated with  
404 the particle-mesh Ewald method (37). The P-LINCS algorithm (38) was used to constrain  
405 bond lengths, and a time step of 2 fs was used throughout. All frames from each simulation  
406 were clustered and the most representative conformations were used as input for molecular  
407 docking (see below). HOP software version 0.4.0 alpha2  
408 (<https://github.com/Becksteinlab/hop>) (39) was used for water molecule dynamics analysis.  
409 Molecular docking calculations were performed using the GOLD software (40) from the  
410 CCDC\_2020 suite and the GoldScore scoring function, with the representative conformers  
411 from molecular dynamics simulations as receptors and the binding sites defined as a 20 Å  
412 radius around the Zn1 ion. All other parameters had default values.

413

## 414 **ACKNOWLEDGEMENTS**

415 We are grateful to Charlotte Huet, Medicine Université Paris-Saclay, LabEx LERMIT, Le  
416 Kremlin-Bicêtre, France  
417 for her technical assistance in the very early stage of the project.

418 We are very grateful to the Prof. Youri Glupczynski, CHU UCL NAMUR for its precious and  
419 highly supportive advices.

## 420 **FUNDING**

421 PSM and MG were supported by financial support from the University of Liege, from  
422 the Belgian Federal Public Service Health, Food Chain Safety and Environment [grant  
423 number RF 17/6317 RU-BLA-ESBL-CPE] and from the Belgian Fund for Scientific Research  
424 (F.R.S.-FNRS) (Grant 35328039).

425 MdB, T-DH, PB, PS were supported by JPIAMR transnational project DesInMBL  
426 Structure-guided design of pan inhibitors of metallo-beta-lactamases Fonds de la recherche  
427 scientifique FNRS N° R.50.01.15.F

428 BII, and EE were supported by the CNRS, Université Paris-Saclay, the Laboratory of  
429 Excellence in Research on Medication and Innovative Therapeutics (LERMIT) through grants  
430 from the French National Research Agency (ANR-10-LABX-33), and by the JPIAMR  
431 transnational project DesInMBL (ANR-14-JAMR-0002).

432 TN, SO were supported by the Assistance Publique-Hôpitaux de Paris, the Université  
433 Paris-Saclay, the Laboratory of Excellence in Research on Medication and Innovative  
434 Therapeutics (LERMIT) through grants from the French National Research Agency (ANR-  
435 10-LABX-33, ANR-17-ASTR-0018), and by the JPIAMR transnational project DesInMBL  
436 (ANR-14-JAMR-0002).

437

438 **TRANSPARENCY DECLARATION**

439 None to declare

440 **REFERENCES**

- 441 1. Theuretzbacher U. 2017. Global antimicrobial resistance in Gram-negative pathogens and  
442 clinical need. *Curr Opin Microbiol* 39:106-112.
- 443 2. Boyd SE, Livermore DM, Hooper DC, Hope WW. 2020. Metallo-beta-Lactamases: Structure,  
444 Function, Epidemiology, Treatment Options, and the Development Pipeline. *Antimicrob*  
445 *Agents Chemother* 64.
- 446 3. Sabath LD, Abraham EP. 1966. Zinc as a cofactor for cephalosporinase from *Bacillus cereus*  
447 569. *Biochem J* 98:11C-3C.
- 448 4. Hansen GT. 2021. Continuous Evolution: Perspective on the Epidemiology of Carbapenemase  
449 Resistance Among Enterobacterales and Other Gram-Negative Bacteria. *Infect Dis Ther*  
450 10:75-92.
- 451 5. Mojica MF, Bonomo RA, Fast W. 2016. B1-Metallo-beta-Lactamases: Where Do We Stand?  
452 *Curr Drug Targets* 17:1029-50.
- 453 6. Lauretti L, Riccio ML, Mazzariol A, Cornaglia G, Amicosante G, Fontana R, Rossolini GM. 1999.  
454 Cloning and characterization of blaVIM, a new integron-borne metallo-beta-lactamase gene  
455 from a *Pseudomonas aeruginosa* clinical isolate. *Antimicrob Agents Chemother* 43:1584-90.
- 456 7. Yong D, Toleman MA, Giske CG, Cho HS, Sundman K, Lee K, Walsh TR. 2009. Characterization  
457 of a new metallo-beta-lactamase gene, bla(NDM-1), and a novel erythromycin esterase gene  
458 carried on a unique genetic structure in *Klebsiella pneumoniae* sequence type 14 from India.  
459 *Antimicrob Agents Chemother* 53:5046-54.
- 460 8. Naas T, Oueslati S, Bonnin RA, Dabos ML, Zavala A, Dortet L, Retailleau P, Iorga BI. 2017.  
461 Beta-lactamase database (BLDB) - structure and function. *J Enzyme Inhib Med Chem* 32:917-  
462 919.
- 463 9. Oelschlaeger P, Ai N, Duprez KT, Welsh WJ, Toney JH. 2010. Evolving carbapenemases: can  
464 medicinal chemists advance one step ahead of the coming storm? *J Med Chem* 53:3013-27.
- 465 10. Borgianni L, Vandenameele J, Matagne A, Bini L, Bonomo RA, Frere JM, Rossolini GM,  
466 Docquier JD. 2010. Mutational analysis of VIM-2 reveals an essential determinant for  
467 metallo-beta-lactamase stability and folding. *Antimicrob Agents Chemother* 54:3197-204.
- 468 11. Franceschini N, Caravelli B, Docquier JD, Galleni M, Frere JM, Amicosante G, Rossolini GM.  
469 2000. Purification and biochemical characterization of the VIM-1 metallo-beta-lactamase.  
470 *Antimicrob Agents Chemother* 44:3003-7.
- 471 12. Garau G, Garcia-Saez I, Bebrone C, Anne C, Mercuri P, Galleni M, Frere JM, Dideberg O. 2004.  
472 Update of the standard numbering scheme for class B beta-lactamases. *Antimicrob Agents*  
473 *Chemother* 48:2347-9.
- 474 13. Garcia-Saez I, Docquier JD, Rossolini GM, Dideberg O. 2008. The three-dimensional structure  
475 of VIM-2, a Zn-beta-lactamase from *Pseudomonas aeruginosa* in its reduced and oxidised  
476 form. *J Mol Biol* 375:604-11.
- 477 14. Lassaux P, Traore DA, Loisel E, Favier A, Docquier JD, Sohler JS, Laurent C, Bebrone C, Frere  
478 JM, Ferrer JL, Galleni M. 2011. Biochemical and structural characterization of the subclass B1  
479 metallo-beta-lactamase VIM-4. *Antimicrob Agents Chemother* 55:1248-55.
- 480 15. Leiros HK, Edvardsen KS, Bjerga GE, Samuelsen O. 2015. Structural and biochemical  
481 characterization of VIM-26 shows that Leu224 has implications for the substrate specificity of  
482 VIM metallo-beta-lactamases. *FEBS J* 282:1031-42.

- 483 16. Salimraj R, Hinchliffe P, Kosmopoulou M, Tyrrell JM, Brem J, van Berkel SS, Verma A, Owens  
484 RJ, McDonough MA, Walsh TR, Schofield CJ, Spencer J. 2019. Crystal structures of VIM-1  
485 complexes explain active site heterogeneity in VIM-class metallo-beta-lactamases. *FEBS J*  
486 286:169-183.
- 487 17. Mojica MF, Mahler SG, Bethel CR, Taracila MA, Kosmopoulou M, Papp-Wallace KM, Larrull  
488 LI, Wilson BM, Marshall SH, Wallace CJ, Villegas MV, Harris ME, Vila AJ, Spencer J, Bonomo  
489 RA. 2015. Exploring the Role of Residue 228 in Substrate and Inhibitor Recognition by VIM  
490 Metallo-beta-lactamases. *Biochemistry* 54:3183-96.
- 491 18. Karampatakis T, Antachopoulos C, Iosifidis E, Tsakris A, Roilides E. 2016. Molecular  
492 epidemiology of carbapenem-resistant *Klebsiella pneumoniae* in Greece. *Future Microbiol*  
493 11:809-23.
- 494 19. Ludden C, Lotsch F, Alm E, Kumar N, Johansson K, Albiger B, Huang TD, Denis O, Hammerum  
495 AM, Hasman H, Jalava J, Raisanen K, Dortet L, Jousset AB, Gatermann S, Haller S, Cormican  
496 M, Brennan W, Del Grosso M, Monaco M, Schouls L, Samuelsen O, Pirs M, Cerar T, Oteo-  
497 Iglesias J, Perez-Vazquez M, Sjostrom K, Edquist P, Hopkins KL, Struelens MJ, Palm D, Monnet  
498 DL, Kohlenberg A. 2020. Cross-border spread of bla NDM-1- and bla OXA-48-positive  
499 *Klebsiella pneumoniae*: a European collaborative analysis of whole genome sequencing and  
500 epidemiological data, 2014 to 2019. *Euro Surveill* 25.
- 501 20. Peirano G, Chen L, Kreiswirth BN, Pitout JDD. 2020. Emerging Antimicrobial-Resistant High-  
502 Risk *Klebsiella pneumoniae* Clones ST307 and ST147. *Antimicrob Agents Chemother* 64.
- 503 21. Pitt ME, Elliott AG, Cao MD, Ganesamoorthy D, Karaiskos I, Giamarellou H, Abboud CS,  
504 Blaskovich MAT, Cooper MA, Coin LJM. 2018. Multifactorial chromosomal variants regulate  
505 polymyxin resistance in extensively drug-resistant *Klebsiella pneumoniae*. *Microb Genom* 4.
- 506 22. Cheng Z, Shurina BA, Bethel CR, Thomas PW, Marshall SH, Thomas CA, Yang K, Kimble RL,  
507 Montgomery JS, Orischak MG, Miller CM, Tennenbaum JL, Nix JC, Tierney DL, Fast W,  
508 Bonomo RA, Page RC, Crowder MW. 2019. A Single Salt Bridge in VIM-20 Increases Protein  
509 Stability and Antibiotic Resistance under Low-Zinc Conditions. *mBio* 10.
- 510 23. Merino M, Perez-Llarena FJ, Kerff F, Poza M, Mallo S, Rumbo-Feal S, Beceiro A, Juan C, Oliver  
511 A, Bou G. 2010. Role of changes in the L3 loop of the active site in the evolution of enzymatic  
512 activity of VIM-type metallo-beta-lactamases. *J Antimicrob Chemother* 65:1950-4.
- 513 24. Rodriguez-Martinez JM, Nordmann P, Fortineau N, Poirel L. 2010. VIM-19, a metallo-beta-  
514 lactamase with increased carbapenemase activity from *Escherichia coli* and *Klebsiella*  
515 *pneumoniae*. *Antimicrob Agents Chemother* 54:471-6.
- 516 25. Docquier JD, Lamotte-Brasseur J, Galleni M, Amicosante G, Frere JM, Rossolini GM. 2003. On  
517 functional and structural heterogeneity of VIM-type metallo-beta-lactamases. *J Antimicrob*  
518 *Chemother* 51:257-66.
- 519 26. Yamaguchi Y, Jin W, Matsunaga K, Ikemizu S, Yamagata Y, Wachino J, Shibata N, Arakawa Y,  
520 Kurosaki H. 2007. Crystallographic investigation of the inhibition mode of a VIM-2 metallo-  
521 beta-lactamase from *Pseudomonas aeruginosa* by a mercaptocarboxylate inhibitor. *J Med*  
522 *Chem* 50:6647-53.
- 523 27. Bogaerts P, Yunus S, Massart M, Huang TD, Glupczynski Y. 2016. Evaluation of the BYG Carba  
524 Test, a New Electrochemical Assay for Rapid Laboratory Detection of Carbapenemase-  
525 Producing Enterobacteriaceae. *J Clin Microbiol* 54:349-58.
- 526 28. Bogaerts P, Rezende de Castro R, de Mendonca R, Huang TD, Denis O, Glupczynski Y. 2013.  
527 Validation of carbapenemase and extended-spectrum beta-lactamase multiplex endpoint  
528 PCR assays according to ISO 15189. *J Antimicrob Chemother* 68:1576-82.
- 529 29. Bogaerts P, Huang TD, Rodriguez-Villalobos H, Bauraing C, Deplano A, Struelens MJ,  
530 Glupczynski Y. 2008. Nosocomial infections caused by multidrug-resistant *Pseudomonas*  
531 *putida* isolates producing VIM-2 and VIM-4 metallo-beta-lactamases. *J Antimicrob*  
532 *Chemother* 61:749-51.
- 533 30. Cornish-Bowden A. 1995. *Fundamentals of enzyme kinetics*. . Portland Press, London.

- 534 31. Pettersen EF, Goddard TD, Huang CC, Couch GS, Greenblatt DM, Meng EC, Ferrin TE. 2004.  
535 UCSF Chimera--a visualization system for exploratory research and analysis. *J Comput Chem*  
536 25:1605-12.
- 537 32. Pronk S, Pall S, Schulz R, Larsson P, Bjelkmar P, Apostolov R, Shirts MR, Smith JC, Kasson PM,  
538 van der Spoel D, Hess B, Lindahl E. 2013. GROMACS 4.5: a high-throughput and highly parallel  
539 open source molecular simulation toolkit. *Bioinformatics* 29:845-54.
- 540 33. Kaminski GA, R.A. Friesner, J. Tirado-Rives, and W.L. Jorgensen. 2001. Evaluation and  
541 reparametrization of the OPLS-AA force field for proteins via comparison with accurate  
542 quantum chemical calculations on peptides. *J Phys Chem B* 105:6474-6487.
- 543 34. Parrinello M, and A. Rahman. 1981. Polymorphic transitions in single crystals: a new  
544 molecular dynamics method. *J Appl Phys* 52:7182-7190.
- 545 35. Hoover WG. 1985. Canonical dynamics: Equilibrium phase-space distributions. *Phys Rev A*  
546 *Gen Phys* 31:1695-1697.
- 547 36. Nosé S. 1984. A unified formulation of the constant temperature molecular dynamics  
548 methods. *J Chem Phys* 81:511-519.
- 549 37. Essmann ULP, M. L. Berkowitz, T. Darden, H. Lee, and L. G. Pedersen. . 1995. A smooth  
550 particle mesh ewald method. *J Chem Phys* 103:8577-8593.
- 551 38. Hess B. 2007. P-LINCS: a parallel linear constraint solver for molecular simulation. *J Chem*  
552 *Theory Comput* 4:116-122.
- 553 39. Beckstein O, N. Michaud-Agrawal, and T. B. Woolf. . 2009. Quantitative analysis of water  
554 dynamics in and near proteins. *Biophys J* 96:601a.
- 555 40. Verdonk ML, Cole JC, Hartshorn MJ, Murray CW, Taylor RD. 2003. Improved protein-ligand  
556 docking using GOLD. *Proteins* 52:609-23.

557

558 **Tables**559 **Table 1: MIC ( $\mu\text{g/mL}$ ) evaluated by broth microdilution of *K. pneumoniae* 20150593, and of its *E. coli* transformant and transconjugant.**

<b>Antibiotics</b>	<b><i>Kp</i> 20150593</b>	<b><i>E. coli</i> TOP10</b>	<b><i>E. coli</i> TOP10 p20150593</b>	<b><i>E. coli</i> J53</b>	<b><i>E. coli</i> J53 p20150593</b>
Temocillin	>128	16	>128	16	>128
Ticarcillin	>512	8	>512	8	>512
Ticarcillin/Clavulanic acid <sup>a</sup>	>256	8	>256	4	>256
Piperacillin/Tazobactam <sup>b</sup>	>256	2	>256	2	256
Cefepime	2	<0.12	0.25	<0.12	0.5
Cefotaxime	>128	<0.12	>128	0.25	128
Ceftazidime	64	0.5	64	1	32
Ceftazidime/Avibactam <sup>c</sup>	>32	0.25	32	0.25	8
Ceftolozane/Tazobactam <sup>b</sup>	>32	0.5	>32	0.5	>32
Ertapenem	16	<0.06	2	<0.06	1
Imipenem	32	0.25	4	0.5	2
Meropenem	16	<0.06	2	<0.06	1
Aztreonam	0.25	<0.12	0.5	<0.12	0.5
Gentamicin	1	<0.5	1	<0.5	2
Tobramycin	8	<0.5	8	<0.5	16
Amikacin	16	<1	16	4	16
Ciprofloxacin	>16	<0.06	<0.06	<0.06	<0.06
Fosfomycin	64	<4	<4	<4	<4
Tigecycline	0.5	0.25	0.12	0.25	0.25
Colistin	>64	0.5	0.5	1	1

560 <sup>a</sup>: clavulanic acid (2  $\mu\text{g/mL}$ ) ; <sup>b</sup>: tazobactam (4  $\mu\text{g/mL}$ ); <sup>c</sup>:avibactam (4  $\mu\text{g/mL}$ )

561 **Table 2: MIC ( $\mu\text{g/mL}$ ) evaluated by broth microdilution of *E. coli* Top 10 pTOPO-VIM-1, pTOPO-VIM-52 and their respective**  
 562 **mutants**

MBLs pTOPO plasmid	Penicillins				Cephalosporins					Carbapenems			Monobactam
	PTZ <sup>a</sup>	TEM	TIC	TCC	FEP	CTX	CAZ	CZA	C/T	ERT	IMP	MER	ATM
No MBL	2	16	8	8	$\leq 0.12$	$\leq 0.12$	0.5	0.5	0.5	$\leq 0.06$	0.125	$\leq 0.06$	0.125
VIM-1	>256	>128	>512	>256	64	128	>128	>32	>32	1	8	4	0.25
VIM-1 H224A	>256	>128	>512	>256	<b>16<sup>b</sup></b>	>128	>128	>32	>32	0.5	8	2	$\leq 0.12$
VIM-1 H224D	128	128	>512	>256	<b>8</b>	64	128	>32	>32	0.25	4	2	0.25
VIM-1 H224K	128	>128	>512	>256	<b>0.5</b>	64	128	>32	>32	1	4	1	0.25
VIM-52	>256	>128	>512	>256	<b>0.25</b>	128	64	32	>32	1	4	2	0.25
VIM-52 S228A	256	>128	>512	>256	0.25	128	32	32	>32	0.5	4	1	$\leq 0.12$
VIM-52 S228D	256	>128	>512	>256	<b>2</b>	64	128	>32	>32	0.25	4	1	0.25
VIM-52 S228K	256	>128	>512	>256	$\leq 0.12$	64	32	32	>32	1	4	1	$\leq 0.12$
VIM-52 S228R	128	>128	>512	>256	$\leq 0.12$	64	<b>16</b>	<b>8</b>	>32	1	4	0.5	0.25

563 <sup>a</sup> PTZ : Piperacillin/Tazobactam (4 $\mu\text{g/ml}$ ) ; TEM : Temocilin ; TIC : Ticarcillin ; TCC : Ticarcillin/ Clavulanate ; FEP : Cefepime ; CTX :  
 564 Cefotaxime ; CAZ : Ceftazidime ; CZA : Ceftazidime/Avibactam; C/T : Ceftolozane/Tazobactam ; ERT: Ertapenem; IMP: Imipenem; MER:  
 565 Meropenem ; ATM: Aztreonam.

566 <sup>b</sup> : important changes are highlighted in bold.

567  
 568  
 569  
 570  
 571  
 572

573 **Table 3: Steady state kinetic parameters for VIM-52, VIM-1H224K.**

574

Antibiotics	VIM-52 (R224)			VIM-1 (H224) <sup>a</sup>				VIM-1 H224K				VIM-2 <sup>b</sup>			
	$k_{cat}$ (s <sup>-1</sup> )	Km ( $\mu$ M)	$k_{cat}/Km$ ( $\mu$ M <sup>-1</sup> s <sup>-1</sup> )	$k_{cat}$ (s <sup>-1</sup> )	Km ( $\mu$ M)	$k_{cat}/Km$ ( $\mu$ M <sup>-1</sup> s <sup>-1</sup> )	<b>R1<sup>c</sup></b>	$k_{cat}$ (s <sup>-1</sup> )	Km ( $\mu$ M)	$k_{cat}/Km$ ( $\mu$ M <sup>-1</sup> s <sup>-1</sup> )	<b>R2<sup>d</sup></b>	$k_{cat}$ (s <sup>-1</sup> )	Km ( $\mu$ M)	$k_{cat}/Km$ ( $\mu$ M <sup>-1</sup> s <sup>-1</sup> )	<b>R3<sup>e</sup></b>
Benzylpenicillin	335±30	130±10	2.6±1.1	29	841	0.034	<b>76</b>	230±20	55±5	4.2±0.5	<b>123</b>	280	70	4	<b>120</b>
Cephalothin	170±20	30±6	5.6±1.8	281	53	5.3	<b>1</b>	200±10	25±6	8±2.3	<b>1.5</b>	130	11	11	<b>2</b>
Ceftazidime	>4.8	>400	0.012±0.002	60	794	0.076	<b>0.15</b>	13±2	340±25	0.04±0.01	<b>0.5</b>	3.6	72	0.05	<b>0.7</b>
Cefepime	>35	>350	0.1±0.03	549	145	3.8	<b>0.026</b>	>12	>500	0.025±0.005	<b>0.007</b>	>40	>400	0.1	<b>0.03</b>
Cefotaxime	120±30	35±5	3.4±0.9	169	247	0.68	<b>5</b>	220±30	40±4	5.5±1.3	<b>8</b>	70	12	5.8	<b>8.5</b>
Imipenem	2.2±0.5	1.2±0.3	1.8±0.7	2	1.5	1.3	<b>1.4</b>	75±15	7.5±0.5	10±2	<b>7.7</b>	34	9	3.8	<b>2.9</b>
Meropenem	0.3±0.1	0.7±0.2	0.45±0.15	13	48	0.27	<b>1.7</b>	1.5±0.1	0.2±0.05	8±0.5	<b>30</b>	5	2	2.5	<b>9.2</b>
Ertapenem	0.3±0.05	0.5±0.1	0.6±0.2	N.D.	N.D.	N.D.	<b>N.D.</b>	1±0.1	0.5±0.1	2±0.6	<b>N.D.</b>	0.2	9	0.02	<b>N.D.</b>

575 <sup>a</sup> Data were from Franceschini et al. (11); <sup>b</sup> Data were from Docquier et al. (25) <sup>c</sup> R1: Ratio  $k_{cat}/Km$  VIM-52/ $k_{cat}/Km$  VIM-1; R2: <sup>d</sup> Ratio

576  $k_{cat}/Km$  VIM-1H224K/ $k_{cat}/Km$  VIM-1; <sup>e</sup> R3: Ratio  $k_{cat}/Km$  VIM-2/ $k_{cat}/Km$  VIM-1.



578 **Table 4. Steady state kinetic parameters for the VIM-52 mutants S228D and S228R**

Antibiotics	VIM52-S228D					VIM52-S228R					
	$k_{cat}$ ( $s^{-1}$ )	$K_m$ ( $\mu M$ )	$k_{cat} / K_m$ ( $\mu M^{-1} s^{-1}$ )	<b>R4<sup>a</sup></b>	<b>R5<sup>b</sup></b>	$k_{cat}$ ( $s^{-1}$ )	$K_m$ ( $\mu M$ )	$k_{cat} / K_m$ ( $\mu M^{-1} s^{-1}$ )	<b>R6<sup>c</sup></b>	<b>R7<sup>d</sup></b>	<b>R8<sup>e</sup></b>
Benzylpenicillin	840±60	84±4	10±2	<b>3.9</b>	<b>294</b>	320±20	16±2	20±4	<b>7.7</b>	<b>590</b>	<b>5</b>
Cephalothin	350±50	30±4	11±3	<b>2</b>	<b>2</b>	500±70	25±3	20±3	<b>3.6</b>	<b>4</b>	<b>1.8</b>
Ceftazidime	>20	>280	0.07±0.01	<b>5.8</b>	<b>1</b>	>2.5	>550	0.005±0.001	<b>0.4</b>	<b>0.06</b>	<b>11</b>
Cefepime	>30	>300	0.1±0.01	<b>1</b>	<b>0.03</b>	>1.5	>320	0.005±0.002	<b>0.05</b>	<b>0.001</b>	<b>0.05</b>
Cefotaxime	270±10	65±8	4±0.6	<b>1.2</b>	<b>6</b>	450±60	50±5	9±2	<b>2.7</b>	<b>13</b>	<b>1.6</b>
Imipenem	2.5±0.4	0.3±0.05	8 ±2.5	<b>4.4</b>	<b>6</b>	20±1	1±0.2	20±5	<b>11</b>	<b>15</b>	<b>11</b>
Meropenem	3±0.2	1.5±0.3	2±0.5	<b>4.4</b>	<b>7.4</b>	0.2±0.04	0.03±0.01	6.6±3	<b>15</b>	<b>25</b>	<b>2.7</b>
Ertapenem	1.8±0.3	2.8±0.4	0.6±0.2	<b>1</b>	<b>N.D.</b>	0.6±0.1	0.06±0.01	10±3	<b>16</b>	<b>N.D.</b>	<b>500</b>

579 <sup>a</sup>R4: Ratio  $k_{cat}/K_m$  VIM-52 S228D/ $k_{cat}/K_m$  VIM-52; <sup>b</sup>R5: Ratio  $k_{cat}/K_m$  VIM-52 S228D/ $k_{cat}/K_m$  VIM-1; <sup>c</sup>R6: Ratio  $k_{cat}/K_m$  VIM-52

580 S228R/ $k_{cat}/K_m$  VIM-52; <sup>d</sup>R7: Ratio  $k_{cat}/K_m$  VIM-52 S228R/ $k_{cat}/K_m$  VIM-1; <sup>e</sup>R8: Ratio  $k_{cat}/K_m$  VIM-52 S228R/ $k_{cat}/K_m$  VIM-2.



582 **FIGURES LEGENDS**

583 **Figure 1. VIM-52 sequence analysis and *bla*<sub>VIM-52</sub> locus characterization.**

584 (A) Multiple alignment of VIM-1 (UniProtKB - Q5GN09), VIM-2 (UniProtKB - Q9K2N0),  
585 VIM-4 (UniProtKB - Q8KRJ3) and VIM-52 (this study). Amino acids positions were  
586 numbered according to the BBL scheme. Positions 224 and 228 are framed. “Z” indicates the  
587 residues interacting with Zn. (B) Class I integron annotation. The 5’CS includes *intl* gene,  
588 while the 3’CS includes the *qacEΔ1*, *sull* and *orf5* genes. The genes cassettes comprise the  
589 following genes: *bla*<sub>VIM-52</sub> (in purple), *aac(6’)-I*, *dfrA1*, *aph(3’)-Ia*. Gene expression are under  
590 the control of a Pc strong (PcS) promoter and a P2 promoter. AttC and attL sites are depicted  
591 in green and in light green, respectively.

592 **Figure 2** Chemical structures of the  $\beta$ -lactam antibiotics used in this study.

593 **Figure 3. Binding site shape variability of the six VIM variants revealed by molecular**  
594 **dynamics simulations.** The proteins are represented as surfaces colored in orange (**a**,  
595 H224/S228), cyan (**b**, K224/S228), brown (**c**, R224/D228), light green (**d**, R224/R228),  
596 purple (**e**, R224/S228) and gray (**f**, Y224/R228), respectively. The zinc ions and the stabilized  
597 water molecules predicted by HOP are represented as mauve and red spheres, respectively.

598 **Figure 4. Stabilizing interactions in the loop 221-241 of the six VIM variants.** The  
599 proteins are colored in orange (**a**, H224/S228), cyan (**b**, K224/S228), brown (**c**, R224/D228),  
600 light green (**d**, R224/R228), purple (**e**, R224/S228) and gray (**f**, Y224/R228), respectively.  
601 The zinc ions are represented as mauve spheres and the hydrogen bonds as black strings.  
602

603 **Figure 5. Molecular determinants for the selectivity of cefotaxime and cefepime on**  
604 **specific VIM variants.** Docking complexes of cefotaxime (**a**, magenta) and cefepime (**b**,  
605 cyan) with the R224/S228 variant of VIM (colored in light green). The zinc ions are  
606 represented as mauve spheres and the hydrogen bonds as black strings.

607 **Figure 6. Molecular determinants for the selectivity of meropenem and benzylpenicillin**  
608 **on specific VIM variants.** The docking complex of meropenem (**a**, dark green) and  
609 benzylpenicillin (**b**, magenta) with the R224/R228 variant of VIM (colored in light green) is  
610 superposed with the H224/S228 variant (colored in orange). The zinc ions are represented as  
611 mauve spheres and the hydrogen bonds as black strings.

**A.**

Signal peptide

50 100

VIM-2 *MFKLLSKLLVYLTASIMAIASPLAFSVDSSGEYPTVSEIPVGEVRLYQIADGVWSHIATQSF DGAVYPSNGLIVRDGDELLLIDTAWGAKNTAALLAEIE*

VIM-4 *MLKVISSLLVYMTASVMAVASPLAHSGEPSGEYPTVNEIPVGEVRLYQIADGVWSHIATQSF DGAVYPSNGLIVRDGDELLLIDTAWGAKNTAALLAEIE*

VIM-1 *MLKVISSLLVYMTASVMAVASPLAHSGEPSGEYPTVNEIPVGEVRLYQIADGVWSHIATQSF DGAVYPSNGLIVRDGDELLLIDTAWGAKNTAALLAEIE*

VIM-52 *MLKVISSLLVYMTASVMAVASPLAHSGEPSGEYPTVNEIPVGEVRLYQIADGVWSHIATQSF DGAVYPSNGLIVRDGDELLLIDTAWGAKNTAALLAEIE*

118 150 196 200 221

VIM-2 *KQIGLPVTRAVST**HFHDDR**RVGGVDVLRAGVATYASPSTRRLAEVEGNEIPHSLEGLSSSGDAVRFGPVELFYPGA**AH**STDNLVVYVPSASVLYGG**CAI***

VIM-4 *KQIGLPVTRAVST**HFHDDR**RVGGVDVLRAGVATYASPSTRRLAEAEAGNEIPHSLEGLSSSGDAVRFGPVELFYPGA**AH**STDNLVVYVPSANVLYGG**CAV***

VIM-1 *KQIGLPVTRAVST**HFHDDR**RVGGVDVLRAGVATYASPSTRRLAEAEAGNEIPHSLEGLSSSGDAVRFGPVELFYPGA**AH**STDNLVVYVPSANVLYGG**CAV***

VIM-52 *KQIGLPVTRAVST**HFHDDR**RVGGVDVLRAGVATYASPSTRRLAEAEAGNEIPHSLEGLSSSGDAVRFGPVELFYPGA**AH**STDNLVVYVPSANVLYGG**CAV***

Z Z Z Z Z

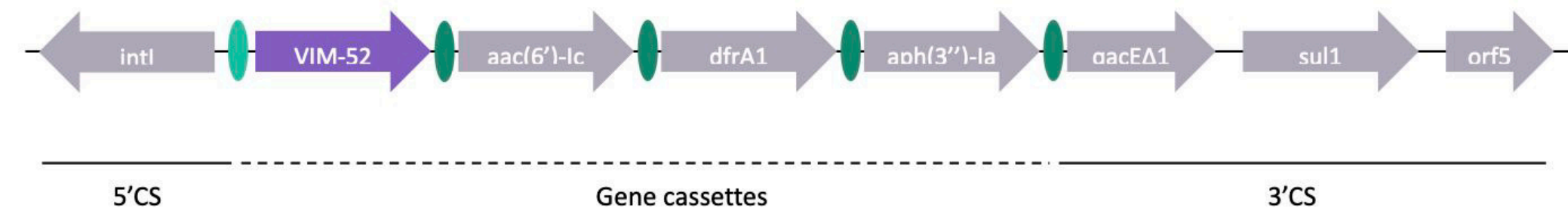
VIM-2 *224 228 **YELSR**TSAGNVADADLAEWPTSIERIQQHYPEAQFVIPG**H**GLPGGLDLLKHTTNVVKAH TNRSVVE*

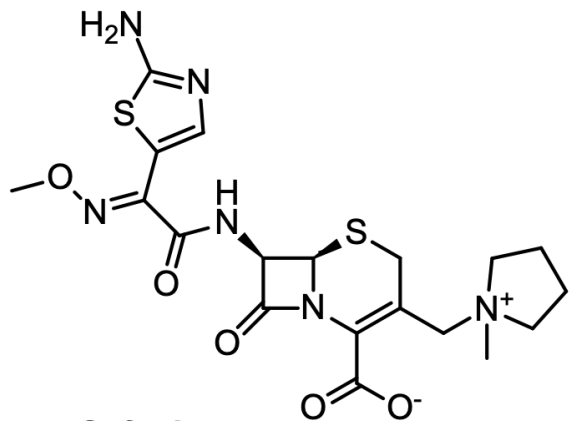
VIM-4 ***HEL**SRTSAGNVADADLAEWPTSVERIQKHYPEAEVVI PG**H**GLPGGLDLLQHTANVVKAHKNRSVAE*

VIM-1 ***HEL**SRTSAGNVADADLAEWPTSVERIQKHYPEAEVVI PG**H**GLPGGLDLLQHTANVVKAHKNRSVAE*

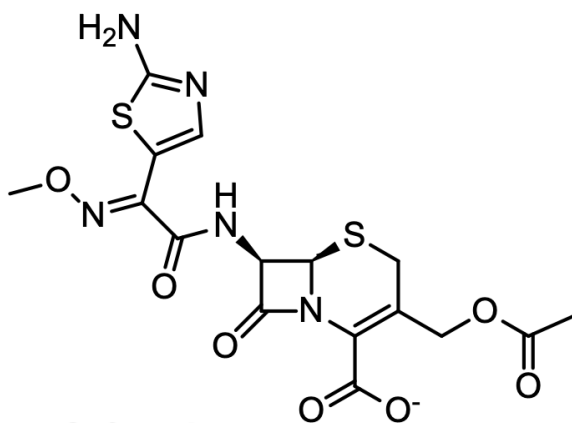
VIM-52 ***REL**SRTSAGNVADADLAEWPTSVERIQKHYPEAEVVI PG**H**GLPGGLDLLQHTANVVKAHKNRSVAE*

Z

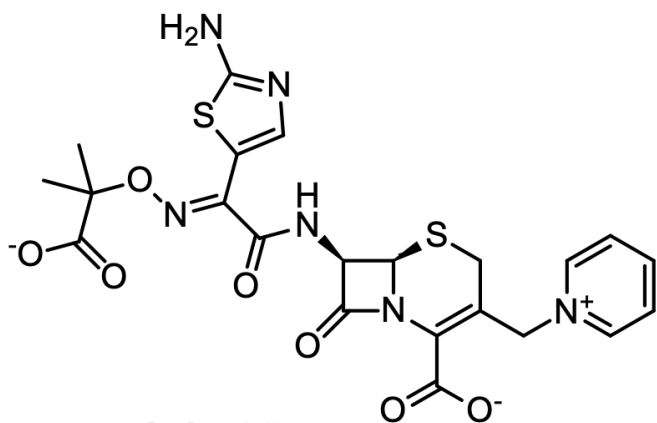
**B.**



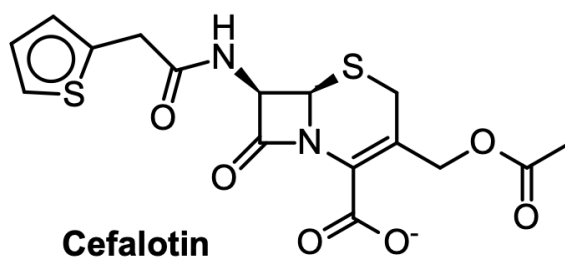
**Cefepime**



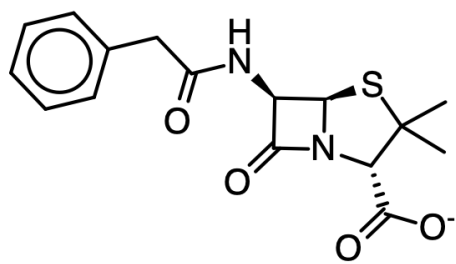
**Cefotaxime**



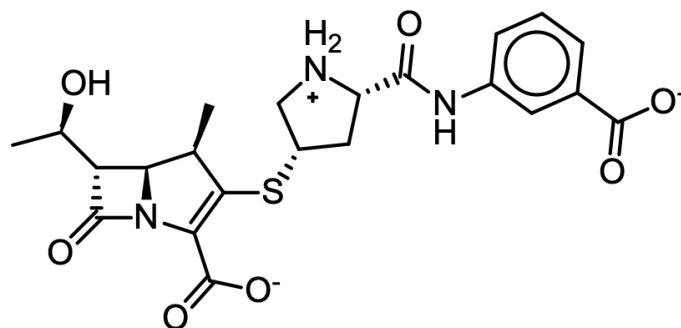
**Ceftazidime**



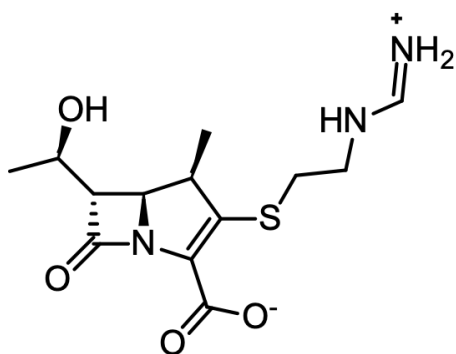
**Cefalotin**



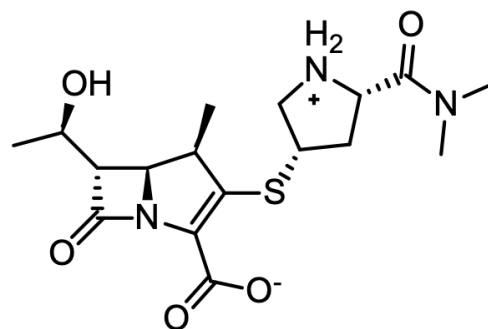
**Benzylpenicillin**



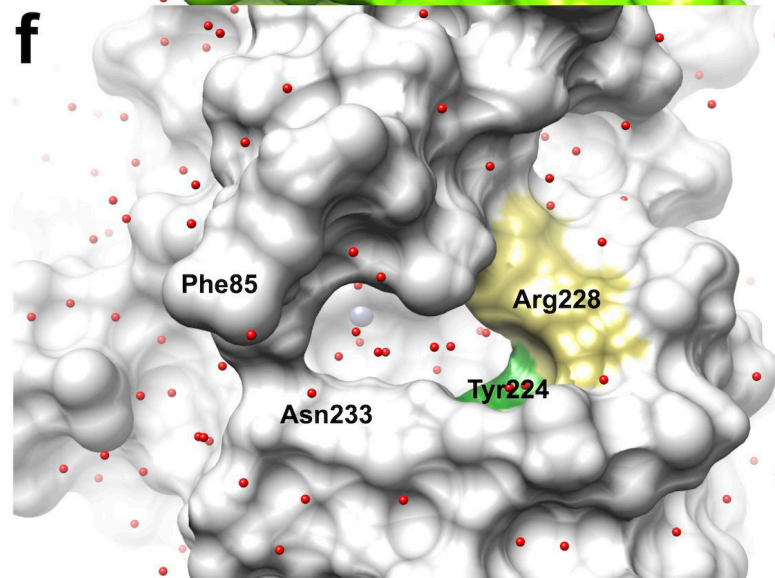
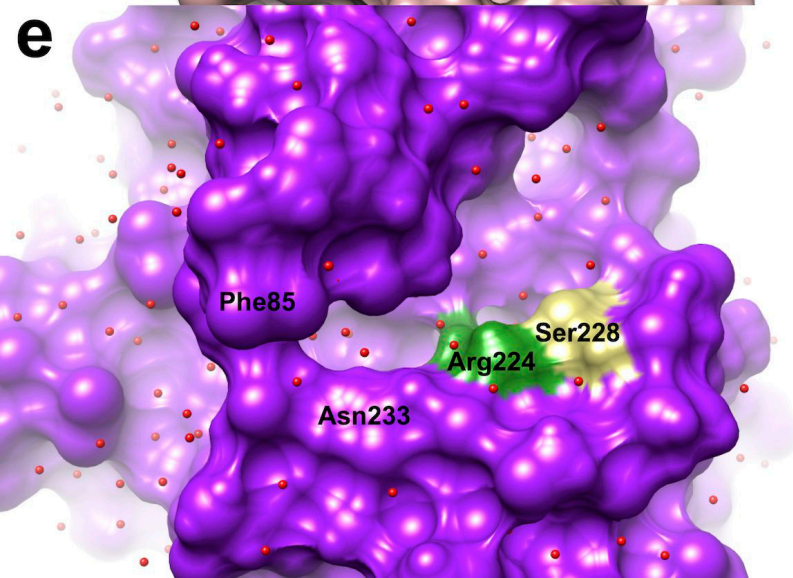
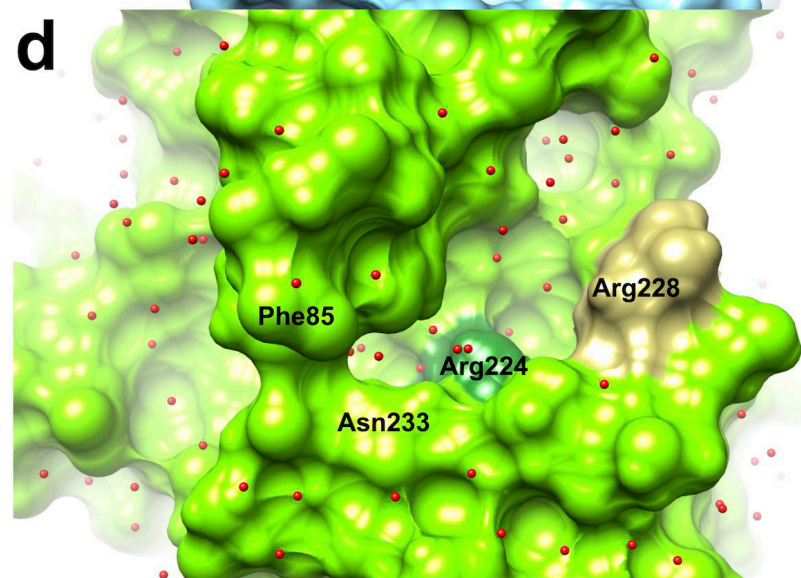
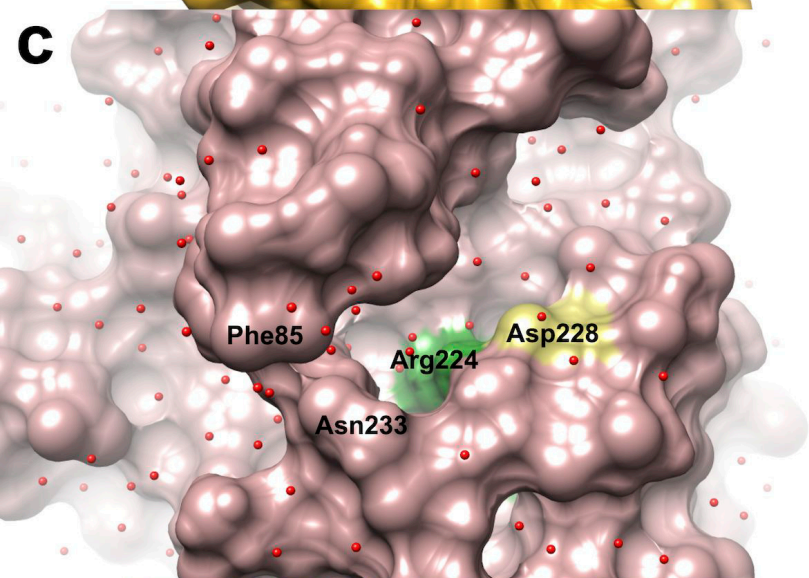
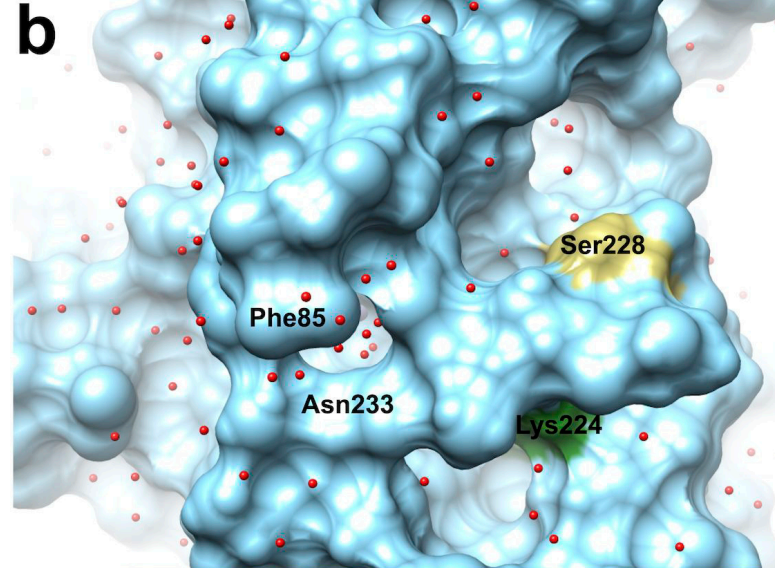
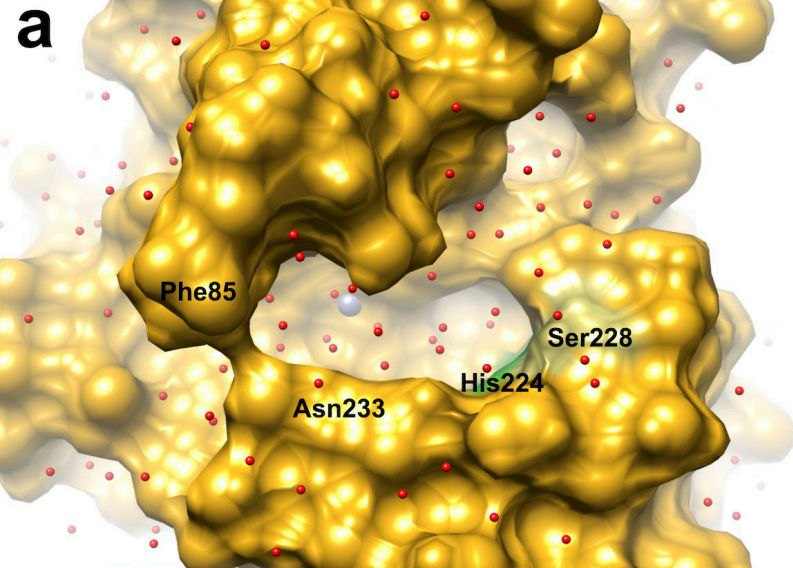
**Ertapenem**

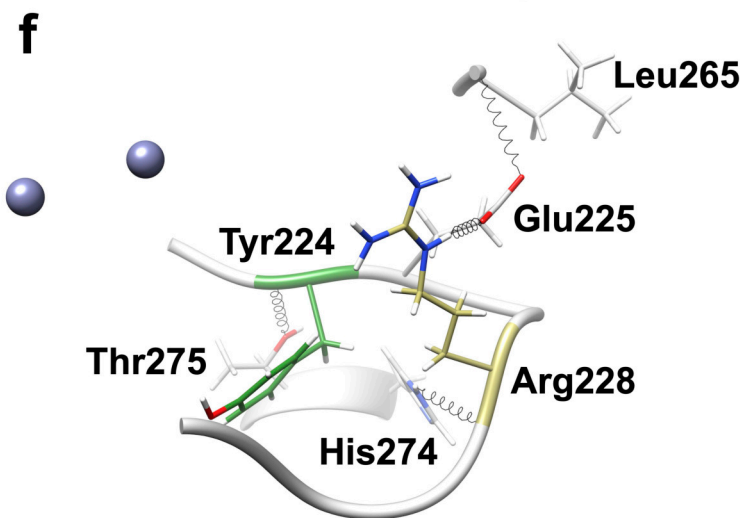
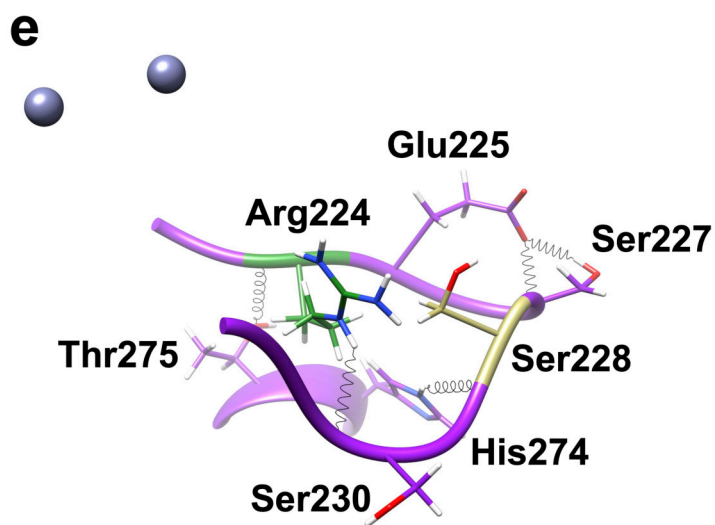
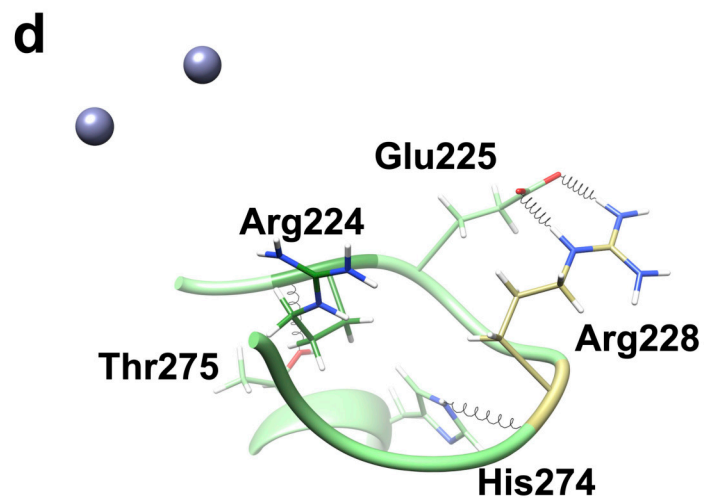
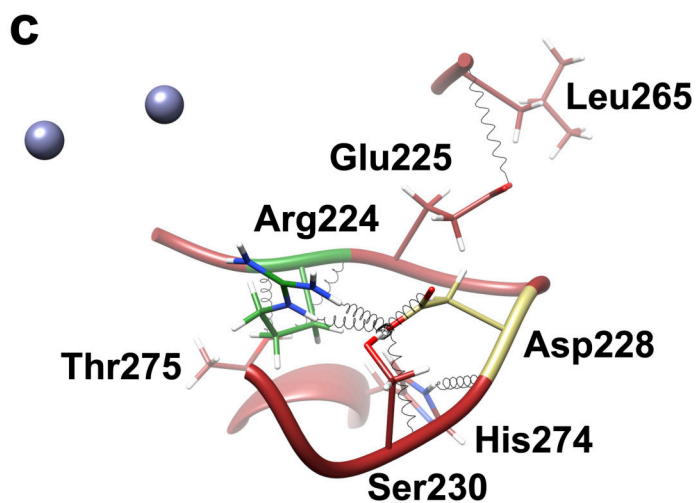
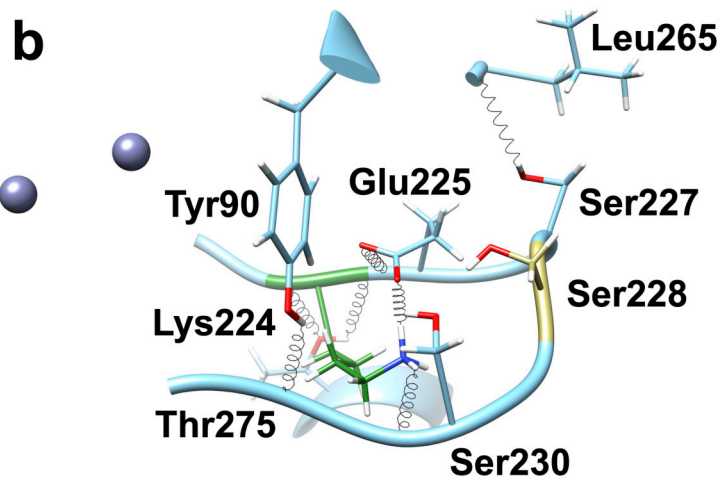
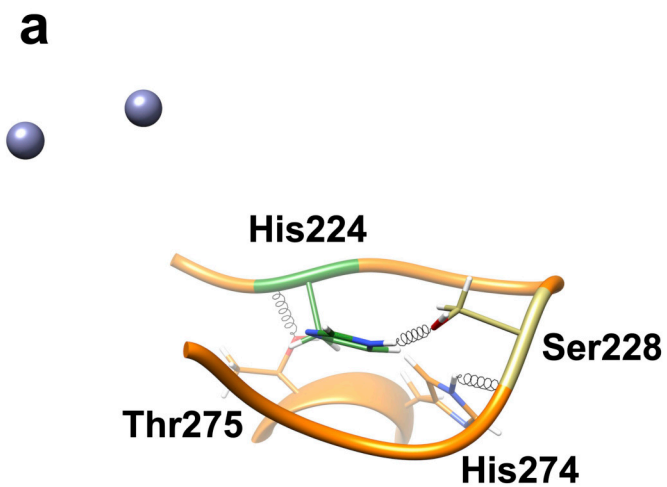


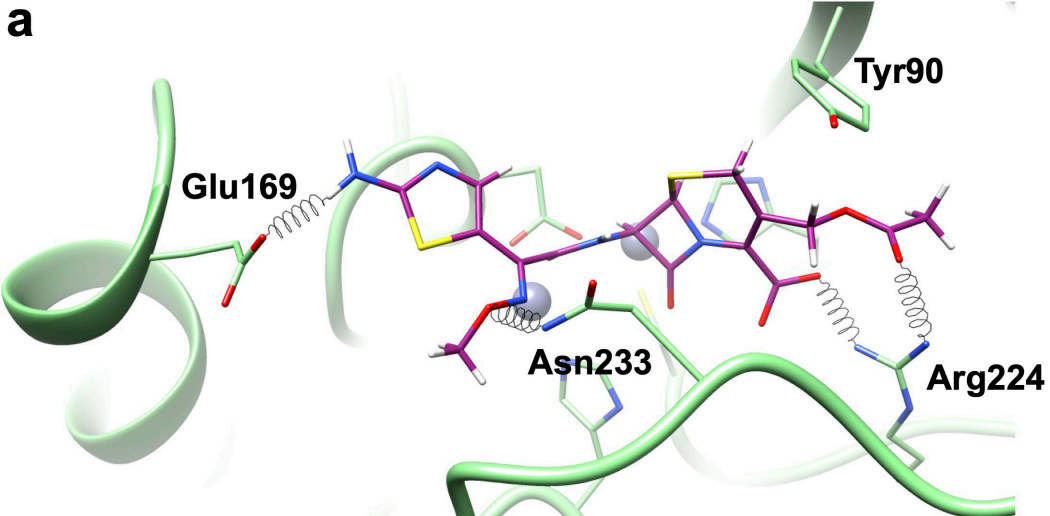
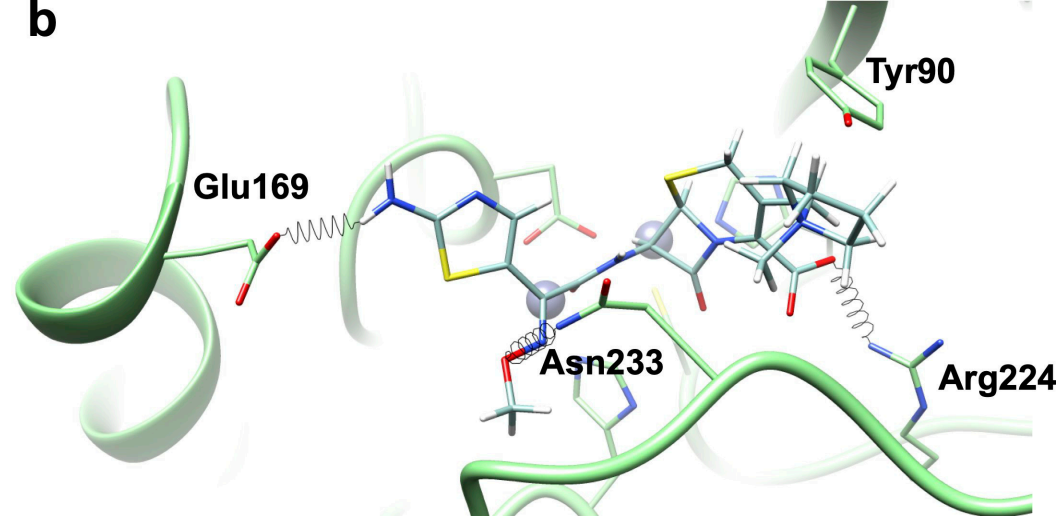
**Imipenem**

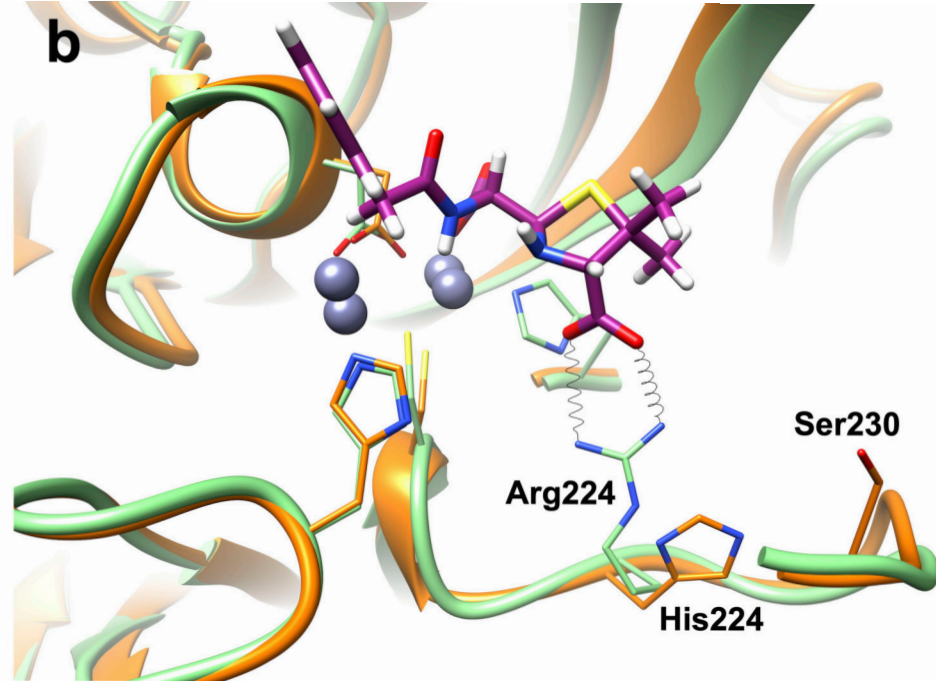
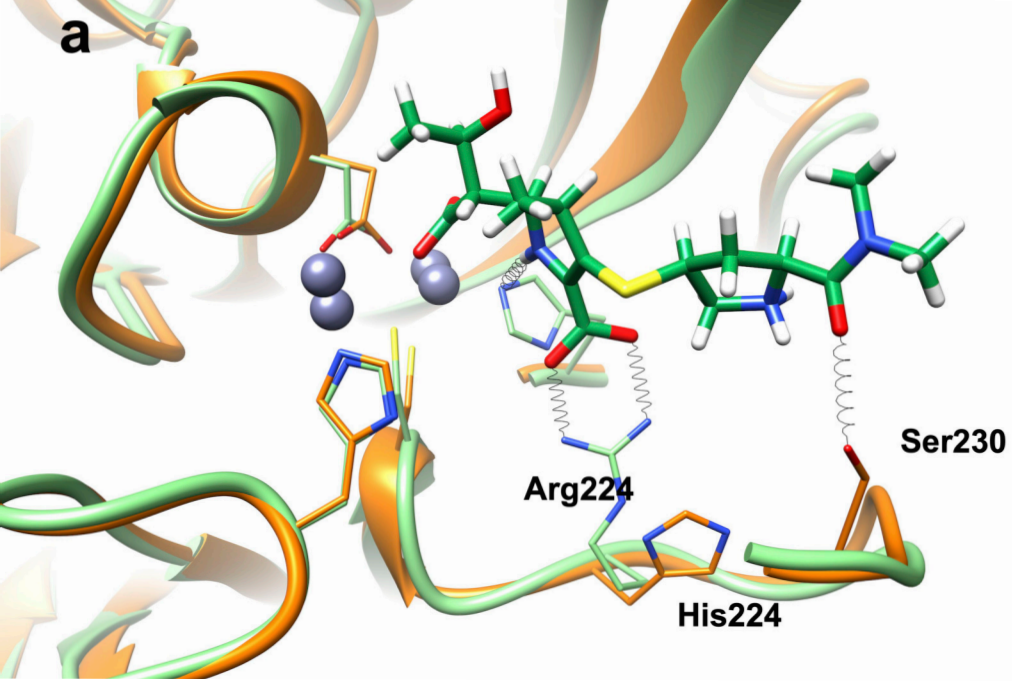


**Meropenem**





**a****b**



**Detection and characterization of VIM-52, a new variant of VIM-1 from**

***Klebsiella pneumoniae* clinical isolate**

Marie de Barsy<sup>a</sup>, Paola Sandra Mercuri<sup>b</sup>, Saoussen Oueslati<sup>c,d,e</sup>, Eddy Elisée<sup>f</sup>, Te-Din Huang<sup>a</sup>,  
Pierre Sacré<sup>a</sup>, Bogdan I. Iorga<sup>f</sup>, Thierry Naas<sup>c,d,e</sup>, Moreno Galleni<sup>b</sup>, Pierre Bogaerts<sup>a</sup>

Supplementary figures S1, S2, and S3

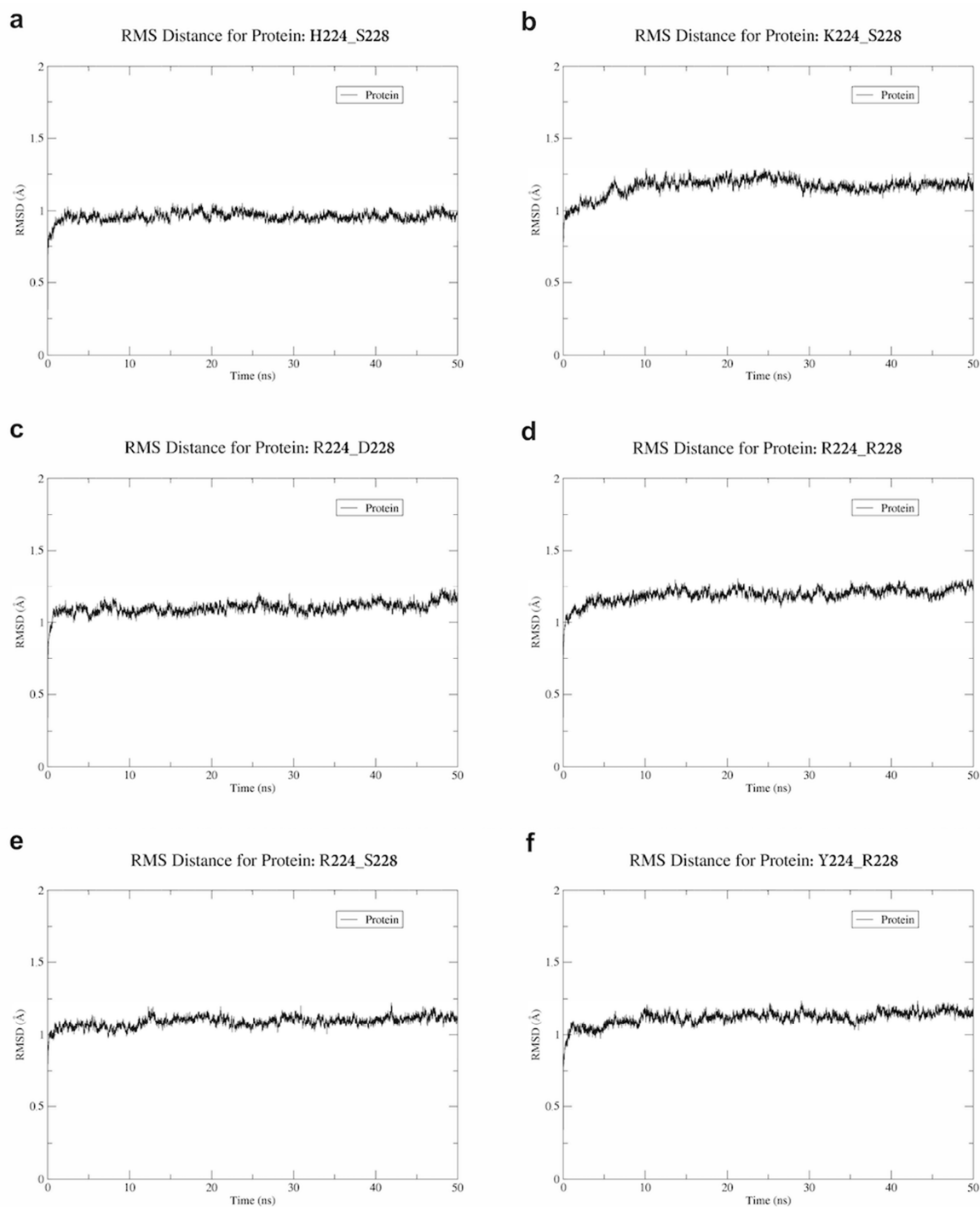


**Figure S1.** Root-mean-square deviation (RMSD) plots from the molecular dynamics simulations of the six VIM variants included in this study: H224/S228 (a), K224/S228 (b), R224/D228 (c), R224/R228 (d), R224/S228 (e), Y224/R228 (f).

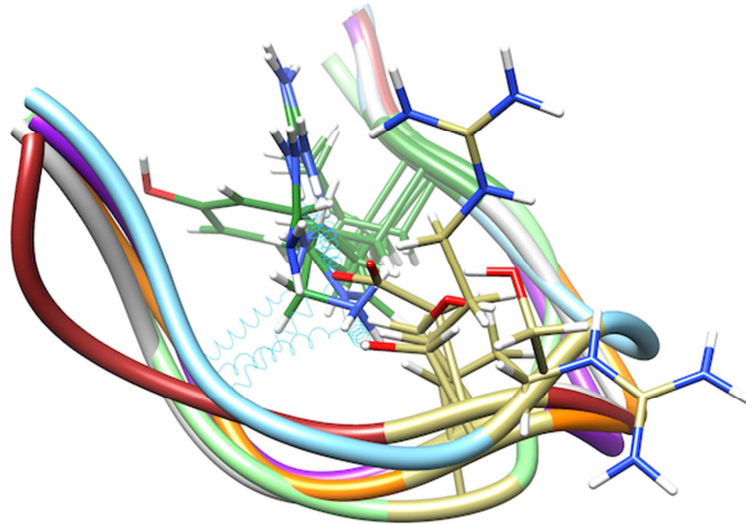


**Figure S2.** Representation of residues 223-232 from molecular dynamics simulations of the six VIM variants included in this study: H224/S228 (orange), K224/S228 (cyan), R224/D228 (brown), R224/R228 (light green), R224/S228 (purple), Y224/R228 (gray). The residues in positions 224 and 228 are represented as sticks colored in dark green and olive, respectively. The hydrogen bonds are represented as strings colored in cyan.

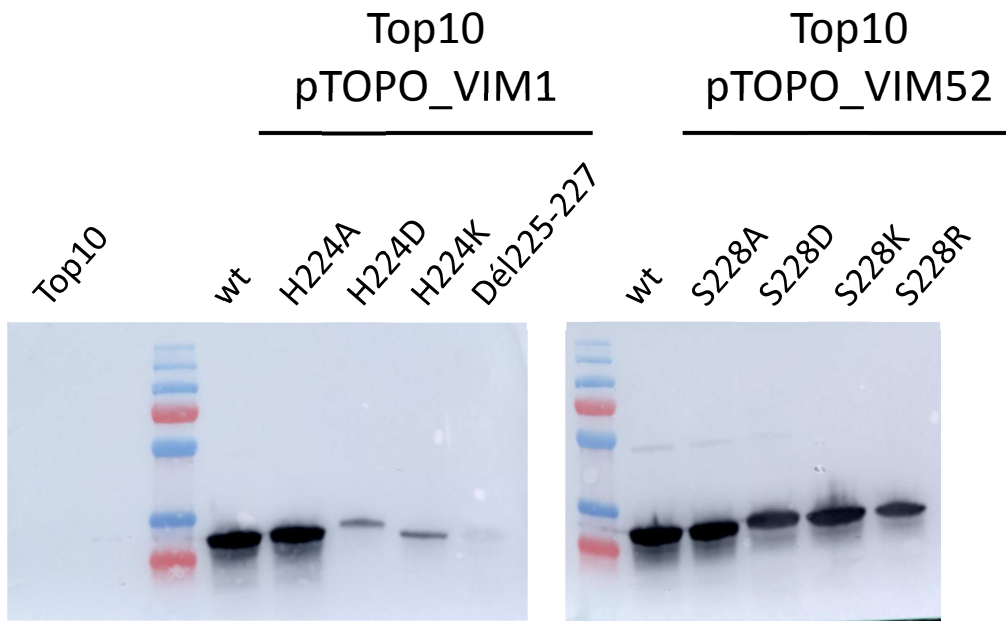


**Figure S3.** Western blot against different mutant of VIM-1 and VIM-52 was performed according to (1) with a mix of 4 rat monoclonal antibodies raised against VIM-2 full. The mutant Del225-227 was not further studied because of instability. The total quantity of protein loaded on the gel was controlled and equivalent between all mutants studied (data not shown).

#### Reference

1. de Barsey M, Jamet A, Filopon D, Nicolas C, Laloux G, Rual JF, Muller A, Twizere JC, Nkengfac B, Vandehaute J, Hill DE, Salcedo SP, Gorvel JP, Letesson JJ, De Bolle X. 2011. Identification of a *Brucella* spp. secreted effector specifically interacting with human small GTPase Rab2. *Cell Microbiol* 13:1044-58.